

Brake Dynamometer Development: Unveiling Precision and Performance

A Technical Report
Presented to the Faculty of the
School of Engineering and Applied Science
University of Virginia

Contributors:
David Mead
Caroline Peterson
Ivan Pudwill
Benjamin Sporysz

Caroline Peterson

May 10, 2024

On my honor as a University student, I have neither given nor received unauthorized aid on this assignment as defined by the Honor Guidelines for Thesis-Related Assignments.

ADVISOR

Michael Momot, Department of Mechanical and Aerospace Engineering

Table of Contents

| | |
|--|-----------|
| 1. Overview..... | 4 |
| 1.1 Formula SAE..... | 4 |
| 2. Introduction..... | 6 |
| 3. Background..... | 7 |
| 3.1 Braking System Overview..... | 7 |
| 3.2 Brake Calipers..... | 9 |
| 3.3 Bias Bar..... | 10 |
| 3.4 Brake Rotors..... | 11 |
| 3.5 Brake Pads..... | 11 |
| 3.6 Pedals..... | 12 |
| 3.7 Hydraulics..... | 12 |
| 3.8 Master Cylinders..... | 13 |
| 3.9 Brake Lines and Fittings..... | 13 |
| 4. Materials Selection..... | 14 |
| 4.1 Brake Rotors..... | 14 |
| 4.2 Bobbins..... | 16 |
| 4.3 Uprights..... | 16 |
| 5. Specifications..... | 17 |
| 6. Screening and Scoring..... | 18 |
| 6.1 Screening..... | 18 |
| 6.2 Scoring..... | 20 |
| 6.3 Justifications..... | 21 |
| Chain Drive Reduction..... | 21 |
| Wheel Speed Sensor For Torque Measurement..... | 22 |
| Frame..... | 22 |
| Brake Pedal..... | 23 |
| 7. Design..... | 23 |
| 7.1 Control System and Sensors..... | 24 |
| 7.2 Frame and Motor..... | 27 |
| 7.3 Simulated Wheel Assembly..... | 29 |
| 7.4 Remote Pedal Assembly..... | 30 |
| Manufacturing..... | 31 |
| 8.1 Waterjet..... | 31 |
| 8.2 Welding..... | 32 |
| 8.3 CNC Mill/Lathe..... | 35 |
| Assembly..... | 37 |
| Results..... | 39 |
| Conclusion..... | 43 |
| References..... | 44 |

| | |
|--|-----------|
| Appendix..... | 46 |
| Appendix A: Bill of Materials..... | 46 |
| Appendix B: Braking System Calculations..... | 47 |
| Appendix C: Rotor Heat Output Hand Calculations..... | 50 |
| Appendix D: Control Loop Code (C++)..... | 51 |
| Appendix E: Serial Receiving and Chart Generation Code (Python)..... | 57 |
| Appendix F: Detailed Drawings..... | 59 |
| Appendix G: Video Demonstration..... | 79 |

1. Overview

1.1 Formula SAE

Formula SAE (FSAE) is a collegiate engineering competition organized by the Society of Automotive Engineers (SAE). The competition allows international teams to design, manufacture, and race open-cockpit, open-wheel, Formula-1 style race cars. Teams such as Virginia Motorsports, the engineering team representing the University of Virginia, are evaluated on their performances in static and dynamic events as depicted in Figure 1.

| Static Events | |
|-------------------------------------|--------------|
| Design Event | 150 |
| Cost & Manufacturing Analysis Event | 100 |
| Presentation Event | 75 |
| Dynamic Events | |
| Acceleration Event | 100 |
| Skidpad Event | 75 |
| Autocross Event | 125 |
| Fuel Economy Event | 100 |
| Endurance Event | 275 |
| Total Points Possible | 1,000 |

Fig. 1: FSAE Competition Score Sheet (*FSAE, n.d.*)

More specifically, teams are judged on their designs, manufacturing methodologies, cost analyses, and ability to articulate and present engineering decisions effectively. This criterion is designated within the category of static events and totals 325 of 1,000 points. The design event is typically considered one of the more significant events. It consists of 10–15 experts within the automotive industry scoring and interviewing students on their design decision-making. The categories in which students are allotted points are designated in Figure 2.

| Category | Areas Covered | Score |
|---|--|--------|
| Suspension o Design o Build o Refinement/Validation o Understanding | Tires, wheels, hubs, uprights, control arms, steering linkage, springs, dampers, anti-roll bars, geometry, kinematics, vehicle dynamics. Selection and use of materials. | ___/25 |
| Frame/Body/Aero o Design o Build o Refinement/Validation o Understanding | Primary structure/tub/tubing, body, and aerodynamic/ductwork systems. Rigidity and stress-relief methods. Load analyses. Fasteners. Selection and use of materials. | ___/25 |
| Tractive/Drive/Recovery System o Design o Build o Refinement/Validation o Understanding | Accumulator(s), Power conversion, Motor/Controller selection/design, Wiring considerations, Transmission. Torque vectoring. Gearing. Regenerative braking. Selection/use of materials. | ___/25 |
| Cockpit/Controls/Brakes/Safety o Design o Build o Refinement/Validation o Understanding | Driver interfaces, seat, belts, steering wheel, steering column, control panel/dash, cockpit sizing & protection, driver comfort/ease of control, pedals, braking system. Is this car as safe as it can be? Selection and use of materials. | ___/25 |
| Systems Management/Integration o Packaging o Electronics/power mgmt o Team Organization o Analysis methods/tools | Design integration, plumbing/wiring, power management, schematics. Are sensitive items protected? Proper use of data? Do systems compliment another? Are progressive project management/ organization methods evident? Special communication tools utilized? What testing/development tools have been used or created? | ___/20 |
| Manufacturability/Serviceability | Ease of repair? Sub-systems accessibility, parts interchangeability, manufacturing complexity? Have fasteners been standardized? Are special tools required to diagnose/service vehicle? | ___/15 |
| Aesthetics/Style | Attractive overall appearance? Is car clean, reflective of professional work? Does car instill team pride, or apologies? | ___/ 5 |
| Creativity | Will this car cause a rules change? Have the judges learned something new? On rare occasions, creative or innovative design may merit special points. | ___/10 |

Fig. 2: FSAE Design Scoring Sheet (*FSAE design score sheet, n.d.*)

It is important to note that within the design vent, a category evaluates the build, refinement/validation, and understanding of the cockpit, controls, and braking systems. This subsystem makes up roughly 17% of the design rubric scoring and demonstrates the importance of a well-rounded and innovative design. The brake system is evaluated in static events and is crucial for passing technical inspection and becoming a top competitor in dynamic events.

The dynamic events, such as skid-pad, acceleration, autocross, and endurance, demonstrate the on-track performance of teams. The skid pad is a figure eight track that evaluates the cornering capabilities of the race cars, and the autocross is a track course that determines the maneuverability of the vehicles. Both of these events demonstrate the aptitude of

the vehicle's suspension. Additionally, acceleration tests the engine's capabilities, aerodynamics, and power transfer from the road to the wheels. Among the events, endurance is arguably the most important as it challenges the vehicle's efficiency, tests the durability of its braking system, and holds the most points in the competition (i.e., 275). As a result, Virginia Motorsports seeks to develop a specialized brake dynamometer to simulate braking forces like those experienced during the dynamic events.

2. Introduction

The role of braking systems in racing goes beyond just decelerating the vehicle. In FSAE, the braking system must provide rapid deceleration capabilities and endurance under extreme temperatures and stresses encountered throughout a race. More specifically, competition braking regulations specify a comprehensive set of rules. The vehicle's braking system must act on all four wheels, employing a single control mechanism capable of locking all four wheels simultaneously. Also, the system must incorporate two independent hydraulic circuits acting on the brake calipers to ensure redundancy if one of the circuits fails. Each hydraulic circuit necessitates its fluid reserve through separate reservoirs or an OEM-style reservoir setup.

Moreover, the brake pedal must be fabricated from steel, aluminum, or titanium and designed to withstand a minimum force of 2000 N without system failure. Non-loadbearing components' failure within the braking system or pedal box should not impede brake pedal operation or the brake system's functionality. Additional requirements exist for electric vehicles (EVs), allowing the first 90% of brake pedal travel for energy regeneration and the remaining travel to directly activate the hydraulic brake system. These regulations underscore the importance of safety, reliability, and technological advancement within the FSAE braking system

guidelines. With an understanding of the brake system's rules, the team can further optimize the braking performance of the formula car.

3. Background

The braking system is designed to decelerate a vehicle in a rapid and controlled manner. This involves constructing a mechanical and hydraulic system to transmit force to the wheel effectively. A brake rotor is directly connected to the wheel, which is acted upon by the brake pads contained within a brake caliper. The brake rotor and pad interaction converts kinetic energy into friction and heat, thus producing the desired deceleration. The caliper's force comes from the hydraulic circuit connected to the master cylinder and brake pedal assembly. With additional components, such as adjustable master cylinders and bias bars, the braking force can be easily modulated by the driver.

3.1 Braking System Overview

Designing an efficient and reliable braking system for a vehicle involves a multitude of engineering decisions. The requirements and desired characteristics of an FSAE car further complicate this design process by introducing even more factors. A key parameter when designing a braking system is the coefficient of friction between the brake pads and brake rotors. The coefficient of friction (CoF) must be a better-understood value and will vary across brake pad materials, rotor materials, shape, and temperature. As the brake pad is applied to the rotor, friction creates heat, changing the CoF and, thus, the available braking force. Figure 3 shows a graph of the CoF vs. time for various brake pad compounds.

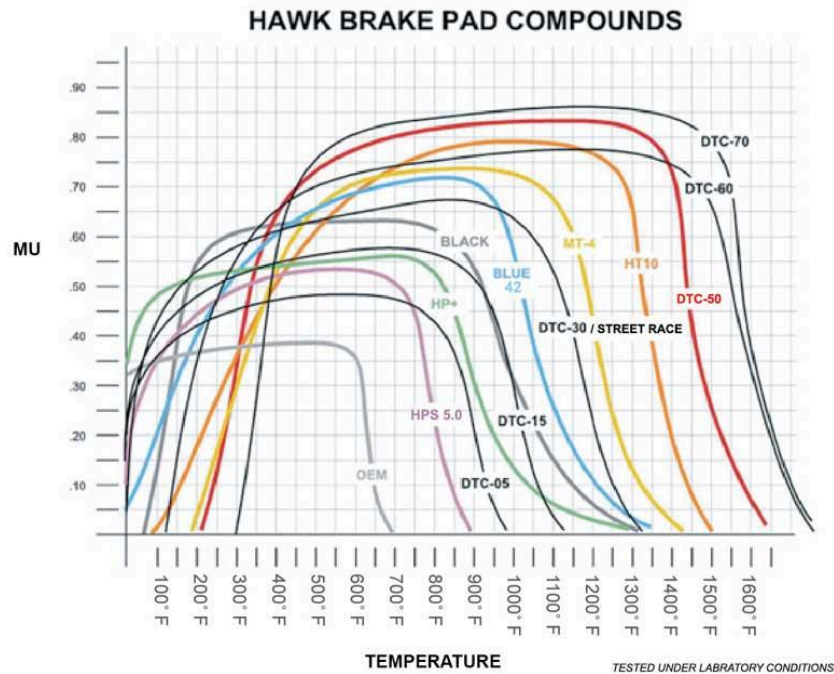


Fig. 3: Hawk Brake Pad Compounds: Coefficient of Friction vs. Temperature (*Hawk Brake Pads - Listed by Compound, n.d.*)

Of note, after the temperature reaches a certain point, the coefficient of friction of the pad drops drastically – a phenomenon called brake fade – a dangerous situation that significantly reduces the braking force and must be avoided. When designing a braking system, it is desired that the brakes operate in the flat, plateau-like region of the curve for optimal performance. The rotor's cooling system must be carefully managed across various speeds and braking conditions to achieve optimal performance. Many parameters can be adjusted to manage the heat created during braking effectively, such as changing the geometry of the rotors by cross-drilling through the rotor or slotting the rotor. Other changes in parameters include changing the rotor material or pad material.

The design process encompasses designing, selecting, and integrating components like calipers, master cylinders, rotors, pads, and the system layout. These components must be meticulously designed to ensure maximum deceleration is available to the vehicle while not losing braking capability throughout a race.

The first step in the design process was the calculation of the system specifications using known parameters such as vehicle weight and velocity. These calculations can be seen in [4. Specifications](#) were completed with the most accurate models possible and drove the design choices for the former braking system. An important note about this process, while it was conducted with a mixture of manufacturer values and estimates, true quantification of the braking system will require measured performance, necessitating the need for a dynamometer.

3.2 Brake Calipers

The brake caliper selection process for the vehicle's braking system involved meticulously evaluating several factors. The Wilwood GP200 brake calipers emerged as the ideal choice due to their lightweight construction, affordability, and performance suitability. Each GP200 caliper, weighing less than 1 lb (0.9 lbs), provided a lightweight option for the vehicle's braking system at a cost-effective rate of \$94.30 per caliper, allowing for an efficient budget allocation across all four wheels.

An essential consideration in caliper selection was the operational pressure range. While Wilwood specified a maximum pressure limit of 1200 psi for the GP200 calipers, a more detailed investigation revealed that this rating was established based on cycle fatigue failure tests at that pressure and might not represent the calipers' ultimate maximum pressure capacity.

Unfortunately, specific engineering data disclosing the ultimate maximum pressure rating for the GP200 calipers was not provided (Wilwood 2023).

However, despite the absence of precise information, the GP200 calipers' compatibility with brake pads ranging from 0.2 to 0.25 inches thick made them a practical choice. The selection was driven by the required clamping force the caliper could produce while using 500 to 1000 psi of brake system pressure. Various caliper specifications like piston orientation and external geometry were also considered, leading to the final selection of the Wilwood GP200 calipers. Its total area, opposed piston layout, lightweight, and pressure limit made it the best choice for the FSAE braking system.

3.3 Bias Bar

Moreover, by utilizing a master cylinder with a 5/8" and 1" bore, we could tune the braking forces at the front and rear of the car. When decelerating, longitudinal weight shift will increase the load on the front tires, necessitating the more significant braking force created with the smaller bore master cylinder. Fine-tune control of the braking system is accomplished by the bias bar. For the 2022-2023 car, the bias bar was adjusted to a ratio of 0.47:0.53 (F: R) to lock both wheels simultaneously. This points to sufficient differences in the bore size of the master cylinders.

Rotor temperatures were carefully considered to maintain consistent brake bias during the endurance event. A temperature difference would alter the effectiveness of the brake pads, changing the braking force. The design focused on aligning the front and rear brake rotor temperatures at a steady state, with front rotors set toward the larger side of the desired range (0.24") and rear rotors towards the smaller side (0.2"). For cost efficiency and material

uniformity, a single large sheet of 0.25" stock was ordered, from which front and rear rotors were machined to their required thicknesses.

3.4 Brake Rotors

In tandem with caliper selection, the rotor diameter was optimized at 9.9 inches for the front and rear brakes. Material selection for the rotors was intricate, aiming to balance pad compatibility, thermal conductivity, strength, and other critical properties. Normalized 4130 steel was the preferred material, displaying an optimal balance of these attributes. The uncertainty regarding the brake pad compatibility with titanium or stainless-steel rotors poses a challenge that will be validated through testing on the brake dynamometer system.

Floating rotors with bobbins made of titanium were chosen to allow automatic centering within brake pads and accommodate thermal expansion. Simulations indicated that increasing the holes in the rotor elevates steady-state temperatures, impacting heating and cooling rates. However, these simulations have limitations related to convection coefficient accuracy, which necessitates further testing for validation.

3.5 Brake Pads

Selecting the appropriate brake pads for racing applications focuses on temperature range, overall friction value, and wear rate. The Wilwood Brake Pad Purple Compound is a composite metallic compound for high-temperature durability on aluminum and other low-conductive alloy rotors. The brake rotors compatible with these brake pads include aluminum, steel, and stainless steel. Since these are compatible with the braking system and future testing mechanisms, these brake pads will also be utilized within the brake dynamometer.

The criteria for pad selection revolve around maintaining adequate friction levels for stopping power within the anticipated temperature range. The temperature and friction force are demonstrated below in the figure.

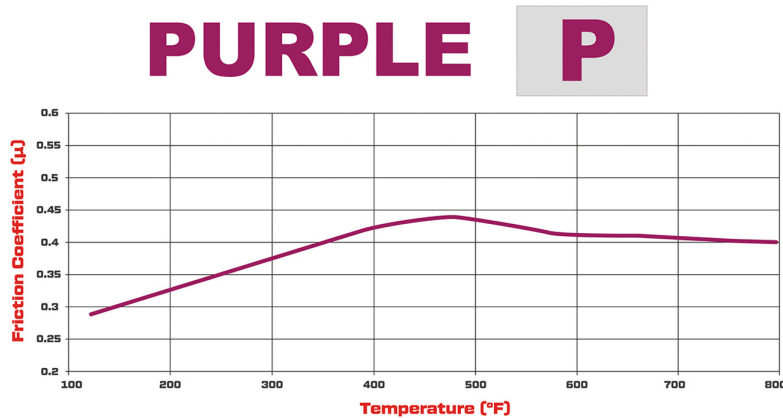


Fig. 4: Temperature (°F) vs. Friction Coefficient (μ) for Wilwood Brake Pad Compound: Purple

3.6 Pedals

The hydraulic system within the braking setup is the pivotal component. Pedal design considerations were also implemented, incorporating curved faces for brake and throttle pedals to optimize driver efficiency, particularly for shorter feet. Adjustable master cylinders and quick-adjust pins for the pedal box were introduced to fine-tune the system for varying driver needs and preferences. These collective efforts exemplify an approach to crafting an efficient and adaptable braking system architecture tailored for FSAE racing.

3.7 Hydraulics

The hydraulic system within the braking setup is the pivotal component responsible for the hydraulically driven actuation and the subsequent application of clamping force at the brake calipers. Encompassing every element within the hydraulic circuit, this system extends from the

master cylinders to the brake calipers, orchestrating the transmission of hydraulic pressure to initiate braking action.

3.8 Master Cylinders

The Tilton 78-Series master cylinders are known for their design and performance in racing applications. These master cylinders offer a range of bore diameters from 5/8" to 1", allowing precise selection to meet the vehicle's braking demands. With a billet aluminum body featuring proprietary low-friction coatings, these cylinders ensure minimal wear while maintaining a lightweight design. Their standout feature is a rear spherical bearing mount and a one-piece piston/pushrod configuration. The structure eliminates side thrust into the master cylinder bore. For the existing configuration of brakes on the FSAE car, a pressure requirement of 450 psi in the rear and 650 psi in the front yielded the appropriate master cylinder bore sizes to maintain uniform forces. The 450/650 ratio resulted in a proportionate front master cylinder bore diameter of 5/8" and a rear bore diameter of 1". The bore ratio is proportional to the ratio of the master cylinder areas given the caliper piston areas and the radii of the rotors. Thus, the bore diameter utilized for the dynamometer is 5/8".

3.9 Brake Lines and Fittings

The hydraulic brake lines, featuring 3-AN 37-degree fittings and steel-braided line construction, efficiently distribute hydraulic brake pressure from the master cylinders. Securely affixed to the chassis via welded tabs, these lines incorporate pressure transducers at t-fittings along the front and rear brake lines. These transducers measure hydraulic pressure within their respective circuits. DOT4 brake fluid with a boiling point of 230 °C ensures system durability

even under extreme temperatures. This setup ensures accurate pressure measurement and effective force distribution within the braking system.

4. Materials Selection

4.1 Brake Rotors

When selecting the best material for the brake rotor testing, several critical attributes for optimal performance under extreme braking conditions were prioritized. The material needed minimal thermal expansion, effective heat dissipation to prevent localized heating, high strength to handle intense braking forces, and a consistent friction coefficient across various temperatures. Initially, materials like carbon fiber were considered, but verifying the strength, thermal expansion, and friction characteristics would require extensive testing. It was also discovered that while titanium was strong, its limited thermal conductivity raised concerns about uneven heat distribution during braking, which could lead to warping or cracking in some rotor regions.

To systematically determine the best brake rotor material, a decision matrix was used to evaluate fundamental material properties such as thermal conductivity, ductility (modulus of elasticity), yield strength, hardness, specific heat capacity, and coefficient of thermal expansion (Figure 4). These properties were prioritized based on their importance to the success of the brake rotor and assigned weights accordingly (Figure 5). Thermal conductivity and ductility were the most critical factors, with weight factors of 3 and 2, respectively, due to their direct influence on heat distribution and rotor integrity. Yield strength, essential for withstanding extreme braking forces, received a weight factor of 2. After evaluating the materials, normalized 4130 steel was found to be the best material, striking the best balance across thermal conductivity, strength, hardness, ductility, heat capacity, and thermal expansion. Since 4130 steel

performs the best and cools the quickest, developing and testing a stainless steel rotor (17-4PH) will be evaluated due to its ability to hold and maintain heat (i.e. low coefficient of thermal expansion) and its very high strength.

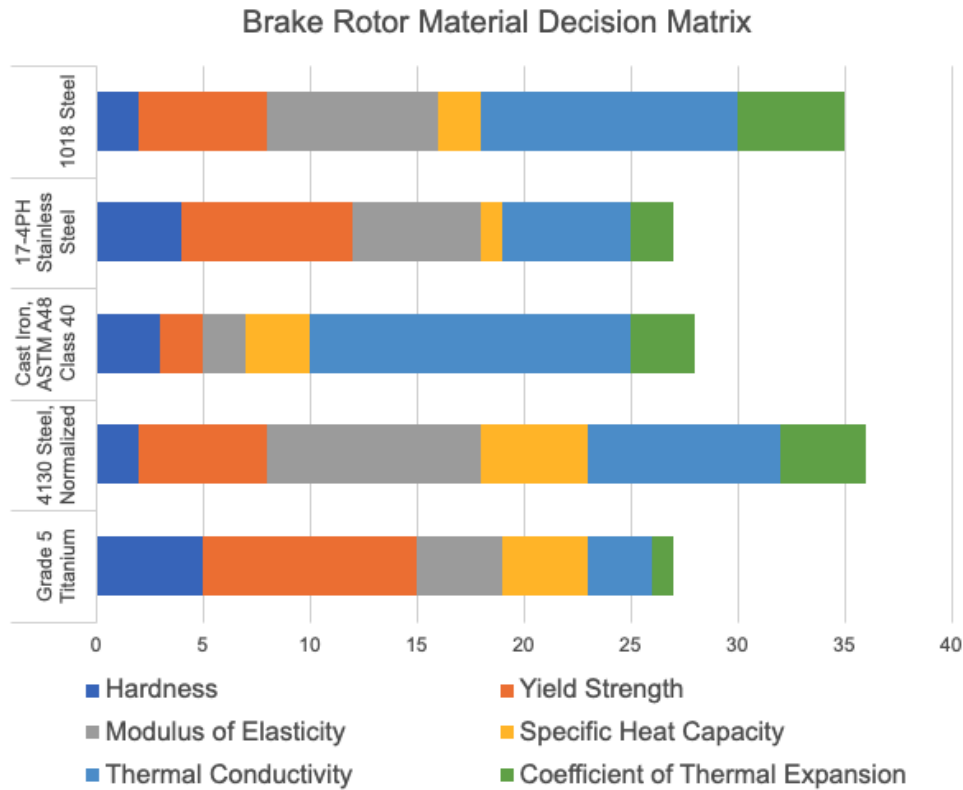


Fig. 5: Brake Rotor Material Design Matrix

The team began validating the models with solid rotors with no holes or slots, as simulations have inherent uncertainties. This approach allowed them to refine the correlation between brake pressure, stopping force, and temperature. The next experimentation stage focuses on finding an ideal rotor design that balances removing thermal mass via drilled holes for enhanced cooling and maximizing the convection coefficient. The aim is to achieve a lightweight rotor with a steady-state temperature appropriate for the brake pads and surrounding components, ensuring optimal performance under varying conditions.

4.2 Bobbins

Grade 5 Titanium was strategically chosen as the material for the bobbins, which are crucial components that attach brake rotors to the hubs within the braking system. This decision was based on the properties of titanium, including its high strength and low thermal conductivity. These properties are essential to withstand the significant forces experienced during braking without risking deformation or stress on the brake rotors. Additionally, titanium minimizes the transmission of excess heat from the steel rotors to the aluminum hubs.

Research into titanium's properties confirmed that anodizing, a standard surface treatment, has little effect on the thermal characteristics of the material. Studies from sources such as Advanced Thermal Solutions Inc. and Wolften indicated that anodizing titanium has negligible effects on its radiative heat transfer properties (Wolften 2021). Therefore, the decision to use titanium for the bobbins was reaffirmed, as it provides reliability under braking stresses while maintaining consistent thermal behavior.

4.3 Uprights

The material for the upright is 7075 T-6 aluminum due to its strength properties, making it the most durable option. Although machined aluminum 6061 is the cheapest and is rated to have adequate machinability, 7075 aluminum surpasses its strength, which is crucial for the structural integrity of the upright. Both 6061 and 7075 aluminum types are amenable to the anodizing process, offering a protective oxide layer after anodization. However, the superior strength of 7075 aluminum, even with a slightly lower machinability rating, makes it the preferred choice for the upright material, ensuring reliability in its structural application.

5. Specifications

Currently, testing and enhancements are made through real-world track testing, which is time-consuming and resource-intensive. Developing a brake dynamometer is essential for determining characteristics necessary for brake evaluation under racing conditions. The dynamometers' design necessitates balancing testing requirements and constraints imposed by real-world racing scenarios. It demands instrumentation capable of measuring various parameters crucial for brake evaluation. The design of the brake dynamometer is driven by the desire to match the braking system design of the 2023-2024 car directly. All key design specifications are driven by the desire to directly match the 2023-2024 car's braking system design. These calculations can be found in [Appendix B: Braking System Calculations](#). To recreate the forces generated by a 300 kg car decelerating at 1.2 g's from 60mph, we must simulate a braking torque up to 135 ft-lbs, a crucial requirement in aligning the testing parameters with the endurance event conditions.

Precise measurement of brake torque and stopping time is fundamental. Instruments are needed to capture torque output and stopping time to correlate with deceleration rates, friction materials' performance, and overall braking effectiveness. Evaluating and controlling input parameters such as pressure and speed control is imperative to recreate race conditions accurately. Assessing brake rotor/pad characteristics, including temperature, wear, distortion, and noise, requires sophisticated instrumentation. Monitoring brake temperatures is necessary to measure wear to ensure longevity and optimal performance.

As briefly mentioned in section 3.1, it is necessary to create a graph of the coefficient of friction (CoF) vs. temperature to design the braking system accurately. This key parameter will influence the braking force and heat produced during braking. An efficient braking system

design will have each brake pad/rotor operating at the temperature at which the maximum braking force is produced. This will increase the vehicle's braking performance, allowing it to decelerate faster, decreasing lap time, and increasing points scored. Beyond parameters like master cylinder bore size, rotor size, brake caliper, etc., the shape of the brake rotor will significantly affect its temperature. Simple hand calculations, as done in Appendix C, can be done to estimate the heat output of the brake calipers.

Additionally, numerical simulations of the brake rotor shape for cooling can be conducted. However, given the complex physical interactions of the brake pads and rotors, they are challenged in producing heat. Additionally, the turbulent airflow generated by the spinning wheel is complex to model accurately, making simulation even more complicated. Thus, building a physical testing system that allows for quick design iterations is easier.

Developing a brake dynamometer that accommodates these diverse measurement requirements while aligning with the constraints of FSAE becomes the cornerstone of this project. Another major constraint on the design of the brake dynamometer is the limited budget of \$700. The dynamometer's design must ensure accuracy in measurement, optimal performance, and, most importantly, safety while balancing cost and manufacturability.

6. Screening and Scoring

6.1 Screening

Initial ideation began by breaking down the dynamometer into four key problems that needed to be solved: drivetrain, torque measurement, frame design, and brake actuation. An initial power delivery architecture of a brushed DC electric motor was chosen at the start of the process due to already having access to a WarP 11 72V motor and a Soliton One motor

controller. Table I demonstrates the 13 different design iterations, or concept variants across all problems, being scored based on the selection criteria.

Table I: Screening and Scoring Concept Classifications

| Concept Class | Letter | Name |
|--------------------|--------|------------------------------|
| Drivetrain | A | Direct Drive |
| | B | Chain Drive |
| | C | Gears |
| | D | Flywheel w/ clutch |
| Torque Measurement | E | Wheel Speed |
| | F | Motor Controller |
| | G | Strain Gages |
| Frame | H | Welded Tube |
| | I | T-slot aluminum |
| | J | Baseplate |
| Brake Actuation | K | Old Pedal Assembly |
| | L | Lever w/ Actuator |
| | M | EV brake booster w/ actuator |

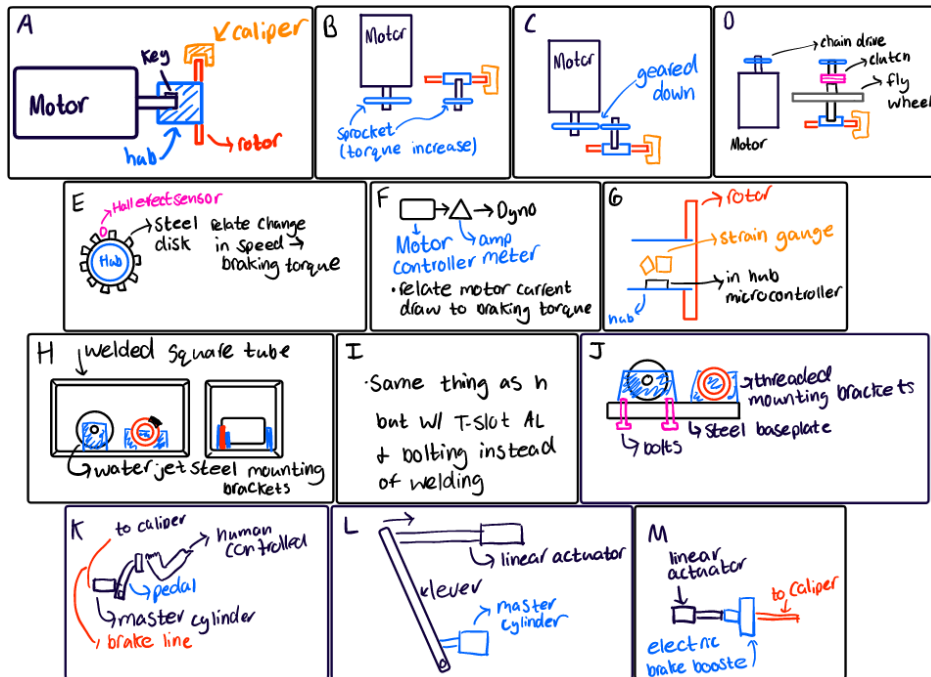


Fig. 6: Ideation

Table II: Screening Criteria and Results

| Selection Criteria | Concept Variants | | | | | | | | | | | | |
|--------------------|------------------|-----|----|----|--------------------|-----|----|-------|-----|----|-----------------|-----|----|
| | Drivetrain | | | | Torque Measurement | | | Frame | | | Brake Actuation | | |
| | A | B | C | D | E | F | G | H | I | J | K | L | M |
| Reliability | 0 | - | - | - | 0 | + | - | 0 | - | 0 | 0 | - | - |
| Engineering Needed | 0 | - | - | - | 0 | + | - | 0 | 0 | - | 0 | - | - |
| Operability | 0 | 0 | 0 | - | 0 | 0 | - | 0 | + | - | 0 | - | - |
| Manufacturing Ease | 0 | - | - | - | 0 | + | - | 0 | + | - | 0 | - | - |
| Safety | 0 | 0 | 0 | - | | | | 0 | 0 | + | 0 | + | + |
| Weight | 0 | - | - | - | | | | 0 | 0 | - | 0 | + | + |
| Torque | 0 | + | + | + | | | | | | | | | |
| Accuracy | | | | | 0 | - | + | | | | 0 | + | + |
| Post Processing | | | | | 0 | 0 | + | | | | | | |
| Pluses | 0 | 1 | 1 | 1 | 0 | 3 | 2 | 0 | 2 | 1 | 0 | 3 | 3 |
| Saves | 7 | 2 | 2 | 0 | 6 | 2 | 0 | 6 | 3 | 1 | 7 | 0 | 0 |
| Minus | 0 | 4 | 4 | 6 | 0 | 1 | 4 | 0 | 1 | 4 | 0 | 4 | 4 |
| Net | 0 | -3 | -3 | -5 | 0 | 2 | -2 | 0 | 1 | -3 | 0 | -1 | -1 |
| Rank | 1 | 2 | 2 | 3 | 2 | 1 | 3 | 2 | 1 | 3 | 1 | 2 | 2 |
| Continue | Yes | Yes | No | No | Yes | Yes | No | Yes | Yes | No | Yes | Yes | No |

From the screening shown in Figure 6 and Table II it was chosen to proceed to the selection stage with ideas A, B, E, F, H, I, K, L. These decisions, at the time, were driven by the desire for a high performing, low complexity system.

6.2 Scoring

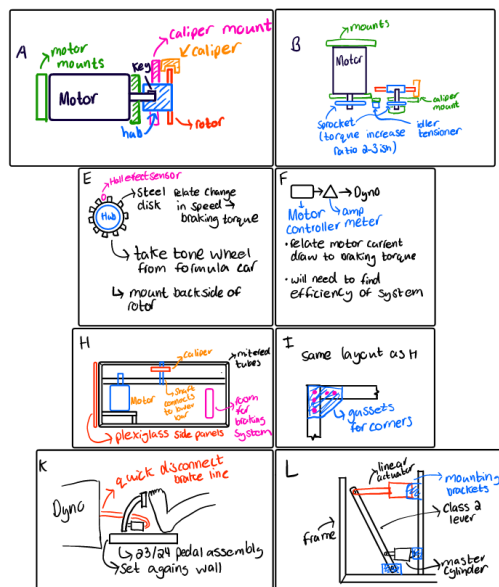


Fig. 7: Concept Classification Ideation

Table III: Selection Criteria

| Concept Variants | | | | | | | | | | |
|--------------------|------------|---------|----------------|---------|----------------|--------------------|---------|----------------|---------|----------------|
| Selection Criteria | Drivetrain | | | | | Torque Measurement | | | | |
| | Weight | A (ref) | | B | | Weight | E | | F (ref) | |
| | | Rating | Weighted Score | Rating | Weighted Score | | Rating | Weighted Score | Rating | Weighted Score |
| Reliability | 10% | 3 | 0.30 | 2 | 0.20 | 10% | 3 | 0.3 | 3 | 0.3 |
| Engineering Needed | 20% | 3 | 0.60 | 2 | 0.40 | 10% | 2 | 0.2 | 3 | 0.3 |
| Operability | 10% | 3 | 0.30 | 2 | 0.20 | 10% | 3 | 0.3 | 3 | 0.3 |
| Safety | 10% | 3 | 0.30 | 3 | 0.30 | | | | | |
| Weight | 10% | 3 | 0.30 | 2 | 0.20 | | | | | |
| Torque | 40% | 3 | 1.20 | 5 | 2.00 | | | | | |
| Accuracy | | | | | | 40% | 5 | 2 | 3 | 1.2 |
| Post Processing | | | | | | 30% | 3 | 0.9 | 3 | 0.9 |
| Total Score | | 3 | | 3.3 | | | 3.7 | | 3 | |
| Rank | | 3 | | 1 | | | 1 | | 2 | |
| Continue | | No | | Develop | | | Develop | | No | |

| Concept Variants | | | | | | | | | | |
|--------------------|--------|---------|----------------|---------|----------------|-----------------|---------|----------------|---------|----------------|
| Selection Criteria | Frame | | | | | Brake Actuation | | | | |
| | Weight | H | | I (ref) | | Weight | K (ref) | | L | |
| | | Rating | Weighted Score | Rating | Weighted Score | | Rating | Weighted Score | Rating | Weighted Score |
| Reliability | 20% | 5 | 0 | 3 | 0 | 10% | 3 | 0 | 3 | 0 |
| Engineering Needed | 10% | 2 | 0 | 3 | 0 | 10% | 3 | 0 | 2 | 0 |
| Operability | 30% | 1 | 0 | 3 | 0 | 30% | 3 | 0 | 5 | 0 |
| Safety | 30% | 4 | 0 | 3 | 0 | 10% | 3 | 0 | 5 | 0 |
| Weight | 10% | 2 | 0 | 3 | 0 | 5% | 3 | 0 | 3 | 0 |
| Torque | | | | | | | | | | |
| Accuracy | | | | | | 35% | 3 | 0 | 5 | 0 |
| Post Processing | | | | | | | | | | |
| Total Score | | 0 | | 0 | | | 0 | | 0 | |
| Rank | | 2 | | 1 | | | 2 | | 1 | |
| Continue | | Develop | | No | | | No | | Develop | |

Based on the selection shown in Figure 7 and Table II a design with a chain driven gear reduction, physical wheel speed sensor, steel tube frame, and an automatically actuated brake pedal was chosen. A short reasoning is given below for the selections.

6.3 Justifications

Chain Drive Reduction

A chain-driven architecture was chosen for several reasons. First, a reduction in motor speed to achieve sufficient torque at a low enough power draw to counteract the braking torque

was needed. This alone ruled out the feasibility of a direct drive. Some additional benefits of doing a chain-drive system include the increased flexibility in packaging all the subsystems. The footprint of the direct drive system would be very long and narrow, making transportation and storage of the brake dyno difficult. This long, narrow footprint would make mounting components like the brake pedal assembly more difficult. Given that we can manufacture custom sprockets, this design also allows us to change the gear ratio of the system cheaply and quickly, depending on our testing requirements.

Wheel Speed Sensor For Torque Measurement

Integrating a hall-effect-based wheel speed sensor into the brake dyno was considered initially to allow for calculating the braking torque from the change in the motor speed; however, this idea was later scrapped in pursuit of a higher accuracy, direct measurement system. However, it was still decided to implement a wheel speed sensor as part of the control system for the brake dynamometer.

Frame

For two reasons, a square-tube 4130 steel frame was chosen over a T-slot aluminum frame. First, given that we have access to the necessary tools to construct it, a tube-steel frame was ultimately cheaper to build than an extruded aluminum frame. Given the same dimensions, a steel frame would be much stiffer than an aluminum frame. A square cross-section was chosen for its manufacturing simplicity.

Brake Pedal

A brake pedal that could be software controlled was selected for multiple reasons:

1. It would ensure high accuracy and repeatability across all measurement runs.
2. It would allow for the simulation of different braking profiles. These profiles can be collected from real-world racing runs, allowing accurate braking simulation.

Creating a software controlled brake pedal increases the end user's safety, removing them from the brake dynamometer while it is running.

7. Design

The physical design of the brake dynamometer can be broken up into multiple significant subsystems: the control system/sensor, the frame and motor, the simulated wheel assembly, and the remote brake pedal. The design of each subsystem was an iterative process, with compliance with the specifications mentioned in section 5 kept as the utmost priority. Detailed drawings of the brake dynamometer design can be found in Appendix F. However, a high-level overview can be seen below in Figure. 8. The packing of each subsystem was driven by the need to have the drive end of the motor in line with the driving end of the brake rotor. With those two systems constrained, other components were located where space allowed.

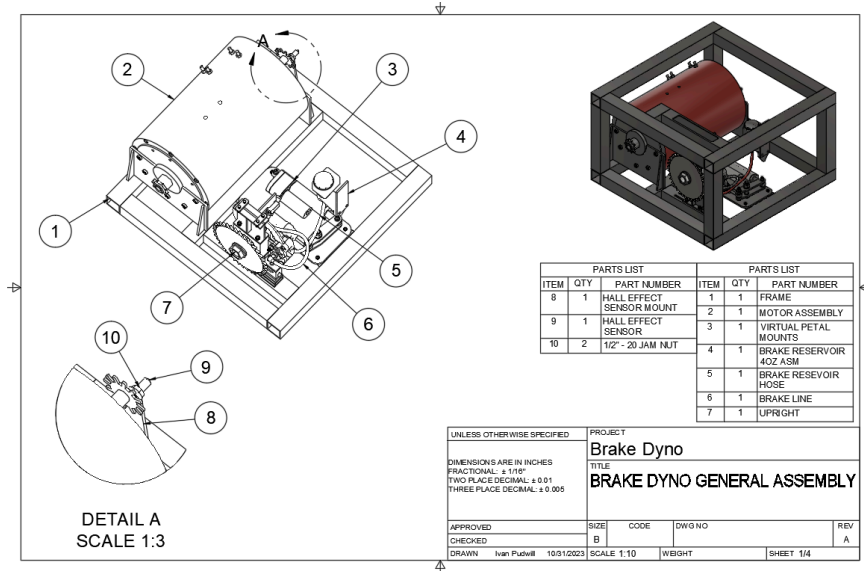


Fig. 8: General Assembly Drawing

7.1 Control System and Sensors

It was first necessary to design the control system, which ultimately dictated what sensors needed to be integrated into the design and how the experiments would be run. Each subsystem's design was driven by our control system's design, which ultimately dictates which factors we can control and measure in the testing of the braking system. The measurement of both variables is necessary to plot the CoF vs. temperature graph. Measuring temperature is simple and can be accomplished by off-the-shelf 16-channel IR-temperature sensors for measuring the temperature of the rotors. Virginia Motorsports already owns several of these sensors, and they are great at what they do. Measuring the coefficient of friction is more complicated. Taking a step back to first principles, it is known that:

$$F_f = \mu N \quad (\text{Eqn. 1})$$

F_f is the braking force, μ is the coefficient of friction, and N is the normal force. The normal force can be calculated from the braking pressure and pad area using the simple equation $P=FA$. Thus, it is necessary to measure the braking force and control the braking pressure to

calculate the coefficient of friction of the brake pads. While it would be possible to apply a set brake pressure, spin the rotor at a constant speed, measure the braking force, and then generate a CoF vs. temperature graph, it was also decided to be able to control the speed of the motor dynamically. This adds additional functionality to the brake dynamometer by allowing rotor cooling studies to be performed. A high-level overview of the brake dynamometer control system can be found in Figure 9.

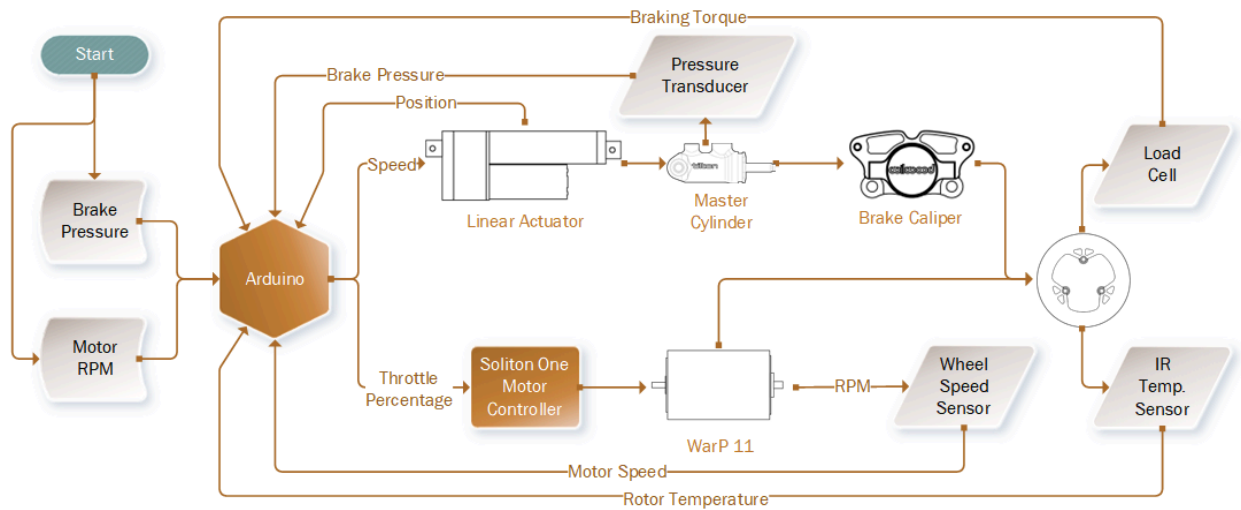


Fig. 9: Brake Dynamometer Control System

Braking pressure can be measured with a pressure transducer directly following the braking system. Virginia Motorsports already owned a Motec pressure transducer. Thus, it will be used for the brake dynamometer. Measuring braking torque is a much more significant challenge. In the initial ideation phase, the braking torque was indirectly calculated from the change in motor/rotor speed or from the motor's current draw. However, these methods were set aside for the increased computational complexity and potential inaccuracies they added. Instead, it was decided to measure the braking torque directly. First, using a pair of strain gauges, a design was created that directly measured the torsion on the wheel hub, the part that connects the sprocket and the brake rotor. This device quickly became quite complicated for two reasons.

First, the device would either have to be self-contained - powering itself and logging its data - or be able to receive power and transmit data through the rotating hub by some slip-ring-like device. Second, the device must operate at high RPMs, withstanding potentially extreme centrifugal forces. An initial iteration of a self-contained hub-insert torque measuring device can be seen below in Figure 10.

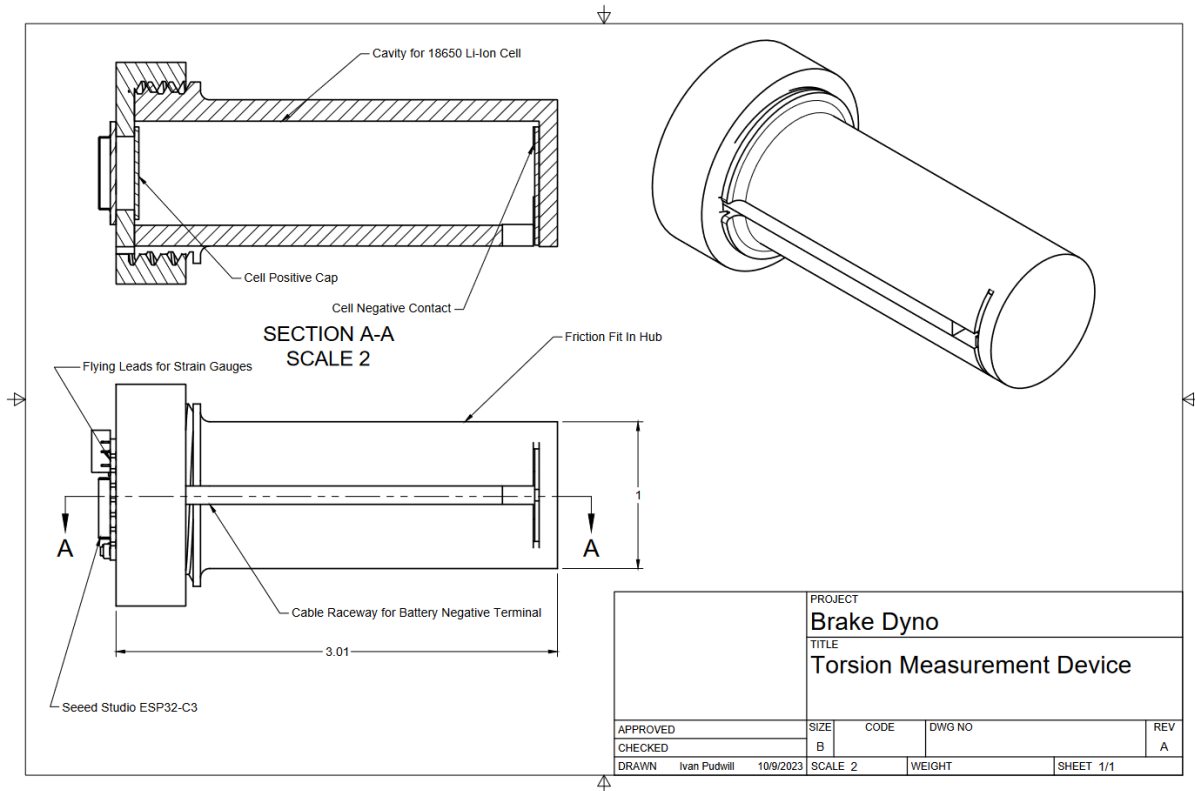


Fig. 10: Torsion Measurement Draft Design

After realizing these complications and a trip back to the drawing board, a new design, consisting of a load cell to measure the reaction forces of the brake caliper, was created. This design, detailed in [Section 7.3 Simulated Wheel Assembly](#), utilizes a load cell in tension or compression (depending on which way the rotor is rotated) to measure the forces imparted on the brake rotor during braking. The braking torque can be calculated from these forces and knowing the radius from the center of the hub to the brake pads.

7.2 Frame and Motor

A square cross-section steel tube frame was chosen as selected in the screen and scoring process. The frame was designed around 2" x 2" x .120 wall low carbon steel tubing. While stronger than necessary, the tubing will ensure the brake dyno's long-term usability across different braking systems, motors, and architectures as the Virginia Motorsports Formula SAE car evolves.

Ultimately, the role of the frame is to mount each subsystem securely. The loading on the frame will be primarily from gravity, reacting to the braking torque and resisting the chain tension between the motor and upright assembly. A rectangular frame was designed to enclose the brake dynamometer fully and allow for the mounting of safety shields on all sides. The bottom members bear most of the structural loads of the frame and will ensure that nothing will leave the dynamometer and potentially injure a bystander in the event of a system failure. The frame was engineered to have four casters on each corner, allowing for the easy repositioning of the dynamometer in the shop; due to budget constraints, these were removed. Nonetheless, there is sufficient structural rigidity in the future to facilitate the addition of wheels.

The Warp 11, weighing in at 230 lbs, will make up the majority of the weight of the brake dynamometer. Two gusseted 3/16" thick steel plates, welded to the tube frame to ensure rigidity, mounted on either end of the WarP 11 motor. Manufacturing and assembly concerns facilitated the decision to mount the Warp 11 motor only using the bottom half of its mounting holes. Thus, the motor mounts are to be fixed to the frame, and the motor is to be lowered from the top of the frame. Because of this modification, it is necessary to check the shear strength of the bolts as they will be reacting to the torque of the motor during operation. The drive side of the motor mounts using 5x 3/8" -16 Grade 8 bolts on an 8.4in bolt circle, and the commutator side mounts

using 5x 5/16" -18 Grade 8 Bolts on a 6in bolt circle. Assuming that both sides of the motor are mounted like the commutator (underestimating the strength of the drive side mounting), as shown in Table IV, even with this modification, it was found that each of the ten mounting bolts will have a safety factor of 35 even under the max torque condition. Therefore, the motor mounting is sufficient.

Table IV: Motor Mounting Bolt Shear Calculations

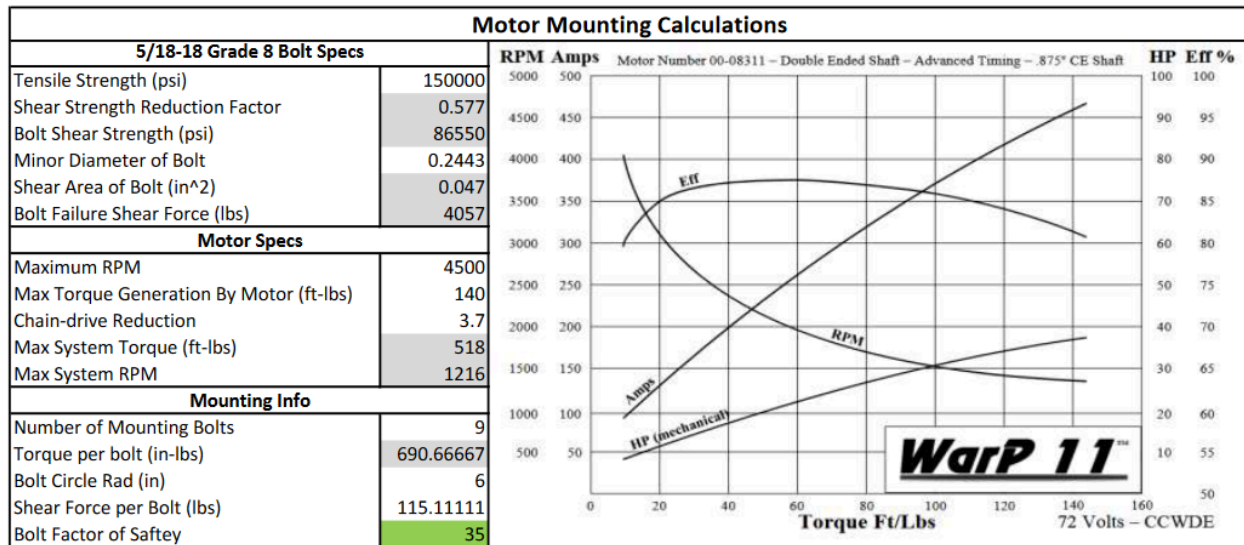


Table IV shows that a final gear ratio of 3.7 was chosen for the brake dynamometer, ensuring that the team will get the maximum torque from the motor and the maximum testing RPM of 1200 (simulating a wheel speed of 60mph). Accordingly, this will minimize the current drawn from the power source. From the final gear ratio, two sprockets were chosen. On the drive side, a ten-tooth sprocket will be used, and on the drive side, a 37-tooth sprocket will be used. The specific tooth count of the sprockets was chosen to maximize chain wrap around the sprockets while ensuring compact packaging in the frame of the brake dynamometer. The sprockets will be connected by the 520 motorcycle chain, which Virginia Motorsports already has experience using.

7.3 Simulated Wheel Assembly

The job of the simulated wheel assembly is multifaceted. It must take the power from the WarP 11 motor and transmit it to the brake rotor while securely mounting the rotor, caliper, and torque measuring device together and to the frame. The design of the wheel assembly was inspired by a typical car wheel assembly, which consists of a hub and upright. Typically, the brake caliper will mount statically to the upright. This is the case for the brake dynamometer, but the mounting method will be modified to accommodate the measurement of the braking torque.

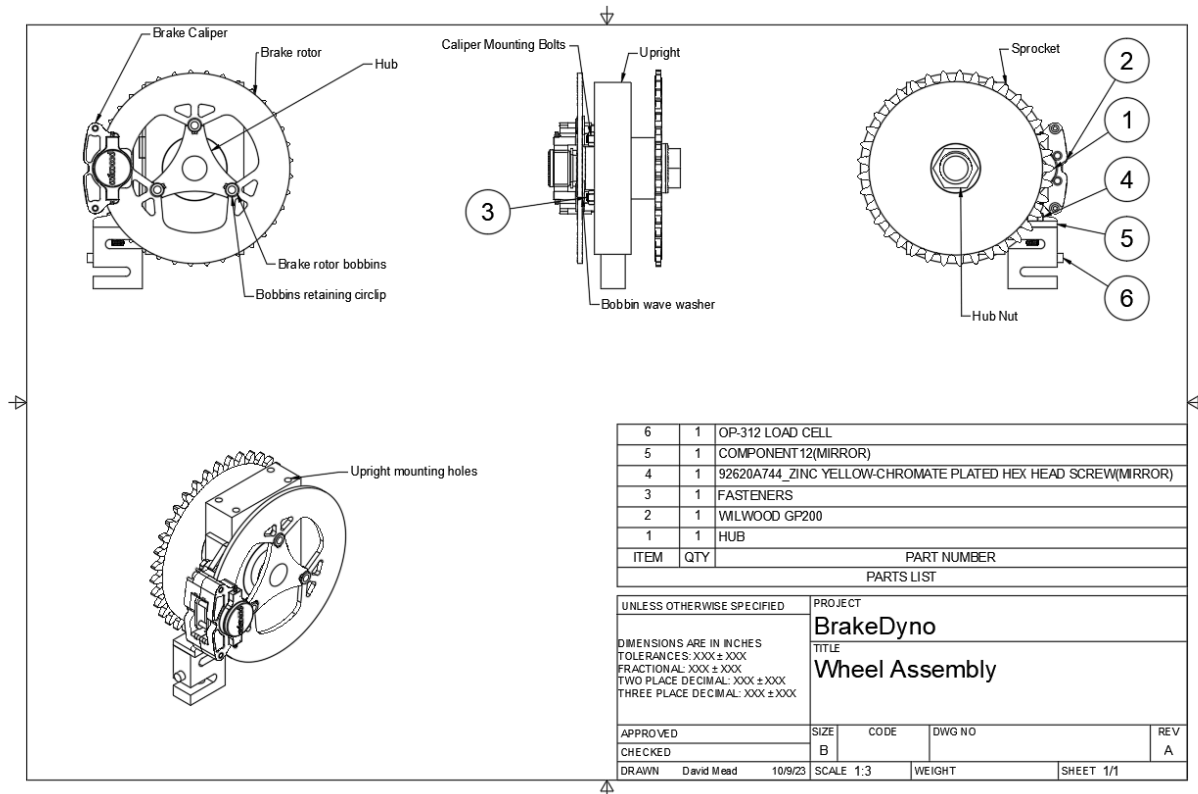


Fig. 11: Fusion design of the wheel assembly.

The upright, shown in Figure 11, attaches the hub to the frame. The upright will hold 2x R24-2Z bearings, rated for the appropriate loads. 2 bearings were chosen to counteract any moments that the uneven loading of the hub might create. The upright will be machined from

7075 Aluminum, primarily because a suitable-sized stock was on hand. It will be mounted on the top and bottom by 8x 5/16"-16 Grade 8 bolts that connect to the two custom I-shaped structures that will bridge the gap between the upright and frame. This arrangement was chosen to reduce the stock size needed for the upright, reducing the overall cost.

The hub design was mostly taken from the 2023 car, with modifications made to support the mounting of the 37-tooth sprocket. It will also be machined from 7075 Aluminum, stock that Virginia Motorsports already has on hand. The load cell will be connected directly to the dynamometer frame and the brake caliper. This will ensure that all braking forces are directly measured. Given a maximum expected braking torque of 135 ft-lbs and an axis of rotation to brake pad radius of 3.4 inches, a load cell with a 1500 lb load rotating was selected. This results in a load safety factor of roughly 3, sufficient to account for any dynamic loading the load cell may experience.

7.4 Remote Pedal Assembly

To generate the braking force, a Tilton 3/16" bore master cylinder was utilized because the team had several of them on hand. Connected in line with the brake line leaving the master cylinder is the Motec pressure transducer. To remotely actuate the master cylinder, a linear actuator was utilized by the team on hand from a previous project. This necessitated using a force multiplier to create the necessary braking pressure. Ultimately, a first-class lever with a 2:1 ratio was selected. This ratio ensured that the linear actuator would operate under its rated load while having sufficient travel to depress the master cylinder completely. The system was mounted on a 1/4" aluminum plate bolted to welded tabs on the brake dynamometer frame. The master cylinder, linear actuator, and lever arm pivot are mounted on cantilevered bolts through

bronze bushings to prevent binding in the system. Figure 12 and [Appendix F: Detailed Drawings](#) overview of the remote pedal assembly.

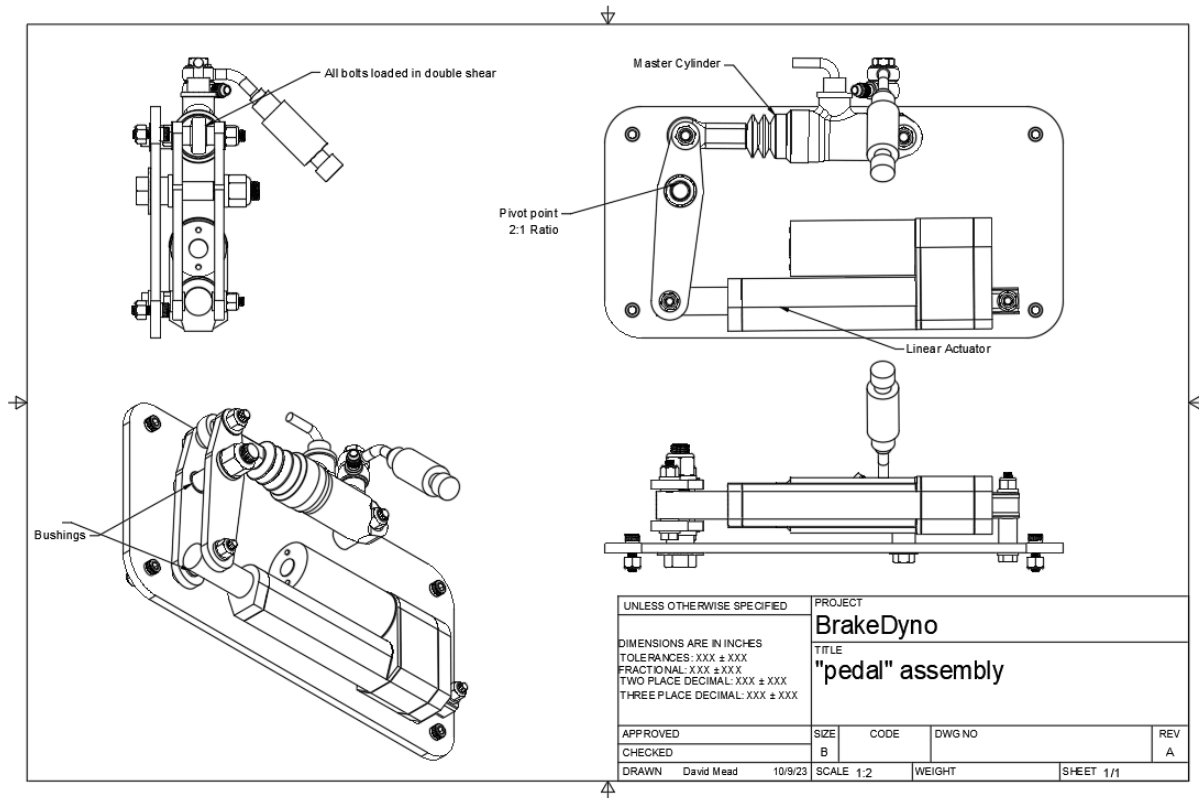


Fig. 12: Pedal Assembly Drawing

Manufacturing

8.1 Waterjet

The square cross-section steel tubing for the frame was manufactured utilizing a waterjet, a versatile machine that uses a high-pressure jet of water with a mixture of an abrasive substance, typically garnet, to cut a wide range of materials such as metal, stone, ceramics, glass, and composites. The jet of water is pressurized to 45,000 pounds per square inch (psi), functioning as the preferred method for cutting materials. The shape of the parts is rendered in Autodesk Fusion 360, where they are then exported as a DXF file (*.dxf) and downloaded to the waterjet software.

Like the steel tubing, the tabs used to secure the linear actuator to the frame, among other components, were cut out of a steel plate. The typical tolerance on the waterjet provided by the university varies based on material and cutting geometry but is estimated to be 0.007” in this case. Keeping this in mind, the hole size for the bolts will include an added tolerance to ensure adequate clearance. The exact process was used for the motor and upright mounts as they possess a simple 2D geometry (Appendix F) with holes to bolt/weld them to their respective parts. Lastly, the drive train sprockets were also manufactured using the water jet and a lathe to chamfer the sprocket teeth.

8.2 Welding

Gas metal arc welding (GMAW), commonly known as metal inert gas (MIG) welding, was used as a fabrication method, melting metals with high temperatures to create fusion. This process involves passing a high voltage through a metal filler wire electrode to heat and fuse the metals under a shielding inert gas. The metal wire electrode is fed through a gun to form the joint, and the shielding inert gas prevents the ambient atmosphere from reacting with the molten metal. The shielding inert gas is a mixture of argon (Ar) and carbon dioxide (CO₂), which creates a more consistent weld by providing better weld pool control and weld spatter minimization. Despite the elevated temperature, the argon (Ar) stays inert throughout welding, enabling easy starts, a stable arc, and shielding from oxidation. The MIG method is a very efficient technique that yields strong joints and attaches brake dynamometer parts to the frame.



Fig. 13: Interior Frame TIG Weld

The frame consisted of 4130 square tubing and was manufactured using gas tungsten arc welding (GTAW), more commonly referred to as tungsten inert gas (TIG) welding. TIG welding requires a non-consumable tungsten electrode and inert gas shielding to achieve high-quality welds. The inert gas utilized, 100% argon, protects and cools the tungsten and weld puddle, similar to MIG welding. However, TIG welding uses a small tungsten rod of various sizes as the electrode. The tungsten can be sharpened to various shapes depending on the welded material. The TIG machine uses a foot-operated variable amperage control, allowing the operator to vary the amperage to the maximum pre-set amperage. When TIG was welding the square tubing for the frame, 120 amps were set as the maximum pre-set amperage. The filler rod (ER120S) diameter was $\frac{1}{8}$ ". It is important to note that the American Welding Society (AWS) has categorized the various alloys and assigned special AWS "ER" numbers to more easily identify the filler materials. ER120S filler is used for various steels where high strength and ductility are critical.

Table V: Filler Rod Selection Size Chart (*Tig Welding Filler Rods, 2024*)

| Metal Thickness (inches) | Filler Rod Diameter (inches) |
|--------------------------|------------------------------|
| 1/16 | 0.045 or 1/16 |
| 3/32 | 1/16 or 3/32 |
| 1/8 | 1/16 or 3/32 |
| 3/16 | 1/8 |
| 1/4 | 3/16 |
| 1/2 | 1/4 |

| Metal Gauge | Joint Type | Tungsten Size | Filler Rod Size | Cup Size | Argon Gas Flow @ 20 PSI (CFH) | Welding Amps | Travel Speed (IPM) |
|-------------|------------|-------------------|-----------------|----------|-------------------------------|--------------|--------------------|
| 1/16" | Butt | 1.6 mm | 1.6 mm | 4, 5, 6 | 15 (7) | 95-135 | 15" |
| | Fillet | | | | | | |
| 1/8" | Butt | 1.6 mm/ 2.4 mm | 2.4 mm | 4, 5, 6 | 15 (7) | 145-205 | 11" |
| | Fillet | | | | | | |
| 3/16" | Butt | 2.4 mm | 3.2 mm | 7, 8 | 16 (6.5) | 210-260 | 10" |
| | Fillet | | | | | | |
| 1/4" | Butt | 3.2 mm | 4.0 mm | 8, 10 | 18 (8.5) | 240-300 | 10" |
| | Fillet | | | | | | |

Regarding the welded joint design of the frame, the geometry was laid out in Autodesk Fusion 360 and jiggged together using magnets and waterjet acrylic braces to maintain the configuration of the frame as initially designed. Important factors in the quality of a MIG weld include the distance from the gun to the weld, the angle between the gun and the weld (15

degrees), the speed of the gun movement, the current, wire feed rate, gas flow rate, and adequate preparation of the piece.

8.3 CNC Mill/Lathe

A large portion of components in the brake dynamometer were CNC machined. The bearing block/upright (Appendix F), hub (Appendix F), and hub nut (Appendix F) are composed of 7075 aluminum, and the brake rotor, made of 4130 steel, was milled. Machining is a manufacturing technique used because of its versatility in achieving complex geometries, tight tolerances, and efficiency compared to other techniques. Fusion 360's CAM software is utilized to program Lacy Hall's CNC milling machine to produce these components. To streamline setup and enhance efficiency, a 5-axis trunnion is employed, granting access to all five sides of the parts in a single setup, significantly cutting down on manufacturing time. Additionally, we will implement high-efficiency milling techniques during programming to minimize excess vibration caused by the geometry of the parts.

The hub was the most difficult-to-machine geometry due to the complex shape of a hexagonal prism with three holes where the midpoint of each lies on the corners, creating "c-shaped" cuts. Another added difficulty of the hub design (Appendix F) is the cylindrical extrusion protruding from the center of the hexagonal prism. This attached cylinder is hollow and possesses external threads on the detached side of the part. Multiple processes were performed to manufacture this as a single component to get the desired design: one lathe setup and two mill setups. The CNC lathe performs precise turning and drilling operations following G-code programming for subtractive manufacturing.

To begin the machining process, the raw material is waterjetted to minimize excess material and enable other parts to be made from the stock that would have otherwise been machined away. The total amount of stock that needed to be removed from the hub required operators to use the lathe and the mill. In the context of the lathe process, the lathe headstock plays a crucial role in holding and rotating the workpiece. It ensures proper centering and provides the power necessary for machining operations. Additionally, the CNC lathe bed provides structural support and must be stiff enough to prevent distortion during operation. The chuck securely clamps the workpiece, allowing for easy loading and unloading. When manufacturing the hub, a three-jaw chuck (universal) was utilized as they are generally stepped on one end to accommodate different sizes of workpieces. The other end is beveled to grip small diameters.



Fig. 14: *Haas* Lathe Setup, Three-Jaw Chuck Rotating the Aluminum Hub.

After using the lathe, the stock material undergoes a precision dovetail cut. This cut enables the 5-axis vise to securely hold and accurately rotate the part in space using its locating pin. The dovetail is machined to a tolerance of ± 0.0005 ". Consequently, the raw material is ready to be loaded onto the 5-axis trunnion table, initiating the machining process. Firstly, large amounts of material from the tops and bottoms of the part should be removed to allow for tool

clearance. Roughing operations utilized heat shrink fit tool holding and high-efficiency machining programming techniques to minimize the risk of vibration and tool chatter, especially important for the long-slender geometry of the hub. This approach aimed to enhance stability and prevent part failure during machining. Subsequently, external finishing passes were executed using a ball nose end mill and an extended length 1/2" end mill to ensure tolerances were met.

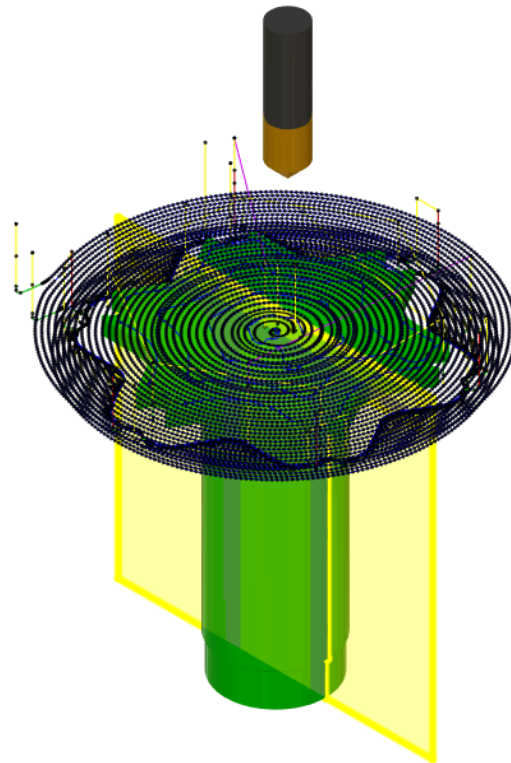


Fig: 15: CNC Tool Path for Hub Design.

Figure 15 illustrates the CNC tool path for the hub design. A second pass over the hub during milling was necessary to flip the piece and achieve symmetrical results on the other side.

Assembly

Once all the components were manufactured, the assembly took place. All the components were designed with features that allow for an efficient assembly process in

accordance with the original Fusion 360 designs (Appendix F). For all critical components, the standard SAE grade 8 fasteners were used. ANSI standard B11.19 was consulted for the design of the chain guarding. Additionally, the 10 and 37 tooth sprockets were both drawn and machined to meet ANSI standard B29.1 for 5-20 roller chains.

The cost of the overall assembly, not including materials and components sourced separately, is approximately \$472.76 (Appendix A). This also does not include the time taken to assemble and manufacture (milling, waterjet, welding) the dynamometer. Using the custom machining quote website Xometry, the estimated cost of the milled parts is \$400. At a larger scale, manufacturing costs could be scaled down by purchasing materials in larger quantities and optimizing machining tool paths.

During the assembly of the brake dynamometer, a couple of aspects were changed in regards to the initial design. Importantly, the initial chain tensioning design was disregarded as the team decided it could negatively impact the strength of the square tubing where the “wheel assembly” mounts. It was decided to initially mount the upright, without slots in the tube and the chain tensioned, and to retrofit a spring loaded chain tensioner later if needed. Another modification to the wheel speed sensor mounting was also made. It was decided to mount the inductive wheel speed sensor so that it read the teeth on the 37-tooth sprocket instead of creating a separate tone ring. This decreased the number of parts that had to be manufactured. Additionally, the dynamometer was assembled mirrored from the CAD design due to an error in the initial motor placement; however, this did not cause any issues with the rest of the assembly.

Results

After the assembly process and before data collection, a preliminary test was conducted to determine the functionality of the brake dynamometer. The initial test run had baseline parameters to determine how the brake dynamometer reacts to a basic. Once the dynamometer was powered on, the wheel speed was programmed to a constant 350 RPM and the brake pressure was set to fluctuate between 10 psi - 75 psi every two seconds. The test run yields crucial data outlining the performance of the brake dynamometer, showcased in Figure 16. This figure illustrates the variation of wheel speed (RPM), brake pressure (PSI), force (lbs), and temperature over the course of 430 seconds.

It is important to note that the results on the graphs have both the non-filtered and filtered values. The data had a lot of noise due to the electromagnetic interference, physical vibration, and the nature of analog signals. To reduce this noise, a low pass filter was applied to eliminate the high frequency data fluctuations from the EMI. Following this, a Gaussian filter was utilized to reduce additional noise and smooth the data from the analog signals in the dynamometer. As shown in the graphs, the filtered data, shown in orange, is significantly smoother than the non-filtered data, shown in blue. This makes fitting curves and collecting meaningful conclusions from the data easier.

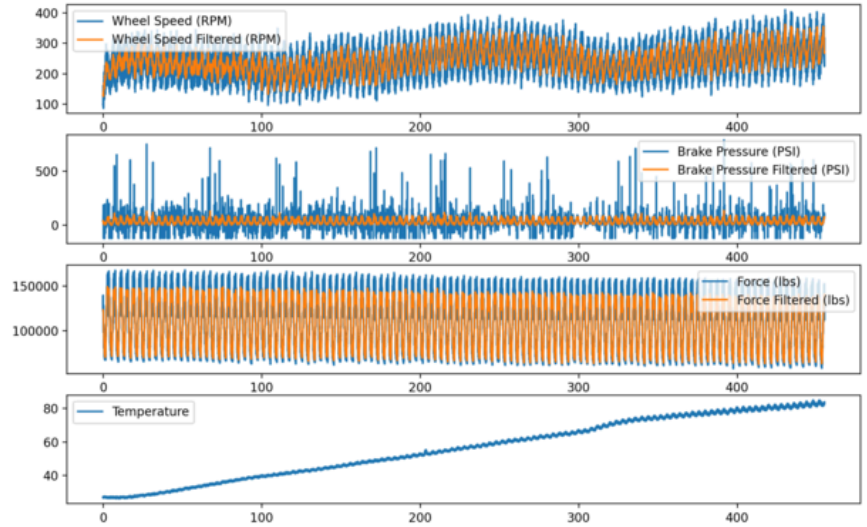


Fig. 16: Preliminary test run for functionality. Graphs depict wheel speed (RPM), brake pressure (PSI), force (lbs), and temperature (°C).

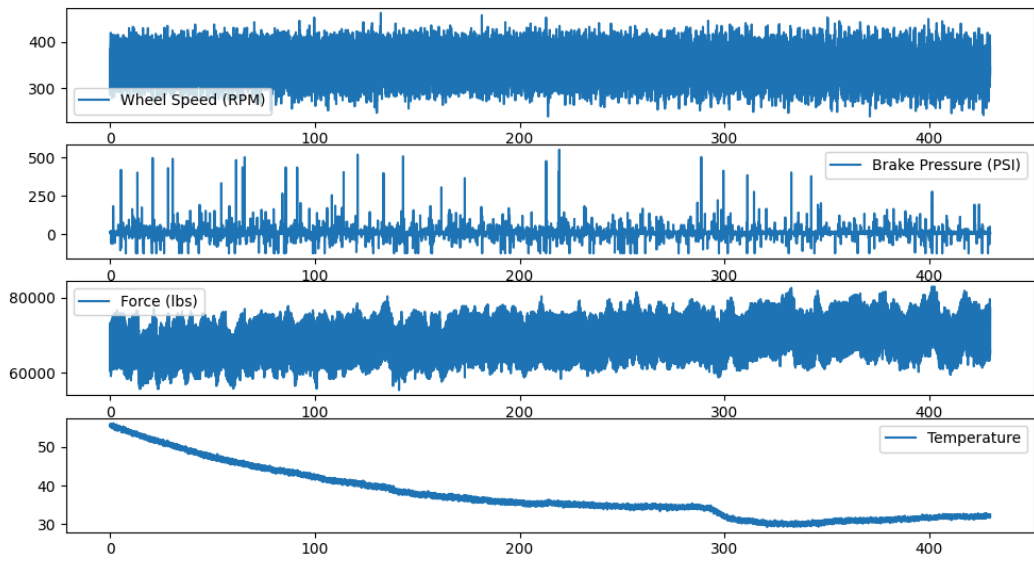


Fig. 17: Cool down of test run for functionality. Graphs depict wheel speed (RPM), brake pressure (PSI), force (lbs), and temperature (°C).

The testing protocol to determine the friction coefficient vs temperature as well as the temperature vs. time curves on the brake dynamometer required specific procedures to yield the desired data. Specifically, we needed to see how the braking torque measured by the load cell

varied with constant braking pressure under different rotor temperatures. Additionally, we also wanted to find the thermal resistance of the rotors by looking at the rate at which the rotor cooled under a constant rpm. We started by spinning the rotor to about 350 rpm and then braking with about 30 psi. The brakes stayed engaged until the rotor hit a target temperature, which in the first run was set to 70°C. Once the rotor hit the target temperature, the brakes disengaged and the rotor spin freely, allowing it to cool (Appendix G). Once it cooled to a target cooling temp, the brakes were engaged again and the cycle continued. The software that controlled this loop can be found in Appendix D.

From this procedure, we were able to see the braking torque across different temperatures as well as the cooling rate from 70 to 60 degrees celsius with multiple trials. Filtering and smoothing was done on the data to reduce noise and fluctuations. From this filtered data, we were able to generate the temperature vs friction curve as well as the temperature vs time cooling curve. The result from this heating and cooling cycle can be seen in Figure 18. A thermal image of the entire system during this run can be seen in Figure 19.

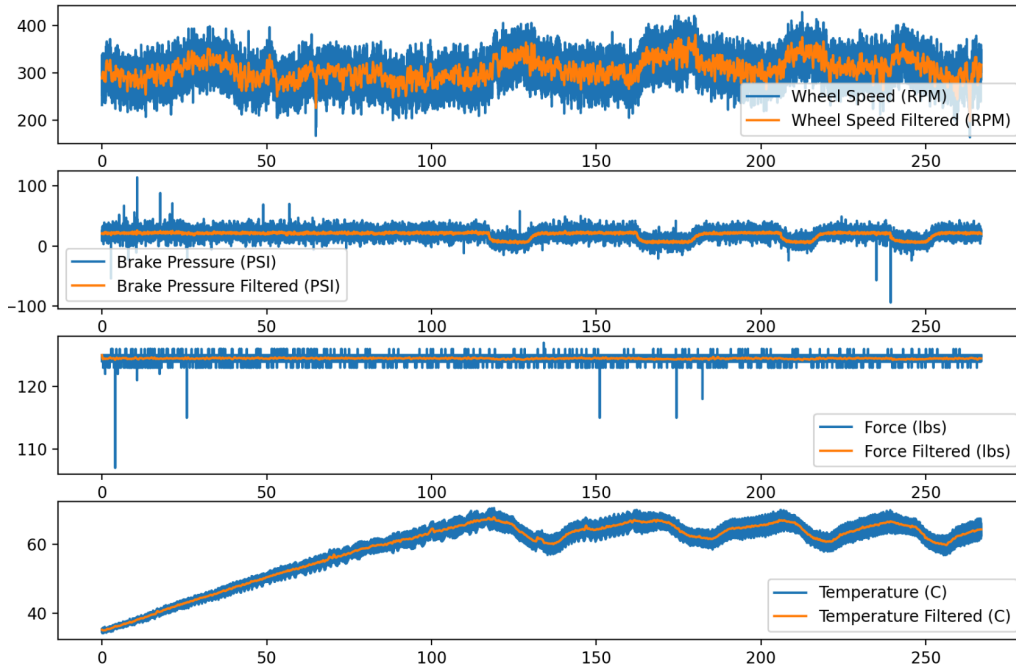


Fig. 18: The figures illustrate the raw data collected after following the testing procedure. Note that the noise is filtered to calculate subsequent values.

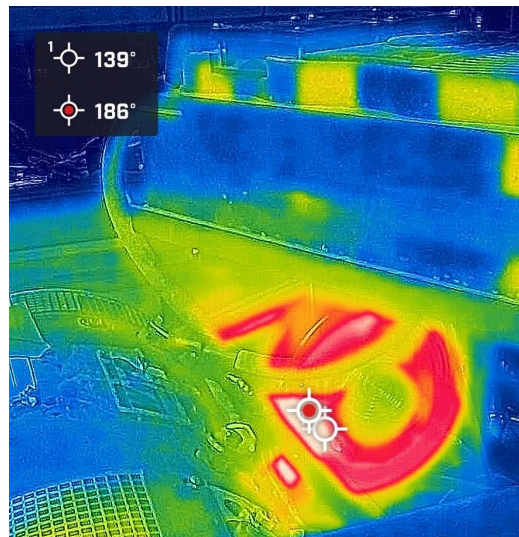


Fig. 19: The figure illustrates the temperature of the brake rotor during testing. The white area is the hottest area on the rotor, which is where the brake calipers are located.

Conclusion

In order to create an ideal braking system for Formula SAE, it is essential to conduct physical testing. To effectively test the braking system quickly, systematically, and comprehensively, it is necessary to create, design, and use a brake dynamometer. As mentioned above, the dynamometer's design encompasses a 3:1 direct drive electric motor capable of simulating up to 135 ft-lbs of braking torque, enabling wheel speeds of up to 60 mph closely matching the real-world braking of Virginia Motorsports FSAE car.

Moreover, the dynamometer aims to simulate the constant 1.2g deceleration of a 300 kg car from 60 mph. Braking torque will be directly measured using a brake caliper load cell. By changing the input parameters of brake pressure and rotor speed, the complex interactions among the different variables of the braking system can be implicated through a carefully designed control system. IR temperature sensors, directly measuring the temperature of the rotor and the braking torque load cell, will be used to construct a coefficient of friction vs. temperature graph for the braking system of Virginia Motorsports 2024 car. This graph is critical to designing a high-performing braking system and is not readily available from manufacturers due to the many variables impacting it.

Through further testing with the brake dynamometer, we expect to reduce the mass of the rotors by about 25%, which will significantly reduce the unsprung mass and rotational inertia of the vehicle, ultimately improving vehicle performance. With proper upkeep, the dynamometer will last for years and continue to provide valuable empirical data while also serving as a test bench for other future experiments.

References

78-series master cylinders. Tilton Engineering. (2023, October 23).

<https://tiltonracing.com/product/78-series-master-cylinders/>

Affordable Electric Vehicle Batteries & components from Electric Car Parts Company. Electric Cars Parts Company. (n.d.).

<https://www.electriccarpartscompany.com/warp-11-ev-dc-motor-72-156v-453a>

2023 FSAE rules V1. FSAE. (n.d.). Retrieved November 15, 2023, from

<https://www.fsaeonline.com/cdsweb/app/NewsItem.aspx?NewsItemID=b9717688-97c4-41f5-b386-74493aad0de6>

FSAE . (n.d.). FSAE design score sheet 150PT. FSAEOnline. Retrieved November 15, 2023, from <https://www.fsaeonline.com/content/FSAE%20Design%20Score%20Sheet-%20150pt.pdf>

Hawk Motorsports. Hawk Performance. (n.d.).

<https://www.hawkperformance.com/compounds/motorsports>

How heat sink anodization improves thermal performance (part 1 of 2 ... (n.d.).

<https://www.qats.com/cms/2010/11/09/how-heat-sink-anodization-improves-thermal-performance-part-1-of-2/>

Tig welding filler rods: Selection size with chart. Weld Guru. (2024, January 4).

<https://weldguru.com/tig-filler-rods/>

Titanium anodizing - wolften, experts in special alloys. WOLFTEN. (2021, March 5).

<https://wolften.pl/en/titanium-anodizing/>

Wilwood disc brakes - brake pad compound: Purple. Wilwood Disc Brakes - Specialty OEM, Racing, and Street Performance Bolt-On Brake Kits. (n.d.).

<https://www.wilwood.com/brakepads/BrakePadsApp?compound=Purple>

Appendix

Appendix A: Bill of Materials

| Part Name | Quantity | Unit Price (\$) | Total Price (\$) | Source |
|---|---------------|-----------------|------------------|---|
| Oil-Embedded Flanged Sleeve Bearing ($\frac{3}{4}$ " | 4 | 1.98 | 7.92 | https://tinyurl.com/Large-Bushing |
| Oil-Embedded Flanged Sleeve Bearing ($\frac{1}{4}$ " | 4 | 1.31 | 5.24 | https://tinyurl.com/Small-Bushing |
| Micro SD Breakout Board | 1 | 3.50 | 3.50 | https://tinyurl.com/Micro-Breakout |
| Load Cell | 1 | 150.00 | 150.00 | https://tinyurl.com/SensorDynasty |
| Motor Driver | 1 | 39.95 | 39.95 | https://www.pololu.com/product/2991 |
| Square Steel Tube | 20 | 5.59 | 111.80 | https://tinyurl.com/Steel-Square-Tubing |
| R24 Bearings | 2 | 47.26 | 94.52 | https://tinyurl.com/Ball-Bearing-R24 |
| HUBX1-1/8 - X Series Weld On Hub 1-1/8" Bore | 1 | 9.22 | 9.22 | https://tinyurl.com/Nitro-HUB-1-8-Bore |
| HUBX1-1/2 - X Series Weld On Hub 1-1/2" Bore | 1 | 9.22 | 9.22 | https://tinyurl.com/Nitro-HUB-1-2-Bore |
| 520 Chain | 1 | 41.39 | 41.39 | https://tinyurl.com/520-Chain |
| Total Cost (\$): | 472.76 | | | |

Appendix B: Braking System Calculations

Imports

```
import math
g = 9.81 # m/s^2
```

System Parameters

Vehicle Parameters

Variable names from Race Car Vehicle Dynamics

```
h = 0.3302 # m
l = 1.5494 # m
M = 300 # kg

weight_distribution_rear = 0.6

a = l * weight_distribution_rear # m
b = l * (1 - weight_distribution_rear) # m

Wfs = (1-weight_distribution_rear) * M * g # N, normal force on front axle (static)
Wrs = weight_distribution_rear * M * g # N, normal force on rear axle (static)

pedal_ratio = 6
```

Master Cylinder Parameters

Tilton 78 series master cylinders

Front: 5/8" diameter bore

Rear: 1" diameter bore

```
# front master cylinder diameter, m
Dmcf = (7/8)*0.0254
# rear master cylinder diameter, m
Dmcr = (1)*0.0254

# front master cylinder area, m^2
Amcf = math.pi*(Dmcf/2.0)**2
# rear master cylinder area, m^2
Amcr = math.pi*(Dmcr/2.0)**2
```

Caliper Parameters

Wilwood GP200 calipers

Carbotech XP8 Pad Compound

```
# Area of caliper piston, m^2
piston_area_front = 2.46 * 0.00064516
piston_area_rear  = 1.566 * 0.00064516

# Effective Caliper Radius, m
caliper_radius_front = 0.09525
caliper_radius_rear  = 0.08

# Pad to rotor friction coefficient (generalized), unitless
u_pad = 0.5
```

∨ Tire Parameters

```
# tire radius, m
tire_radius = 0.2032 # 8 inch radius

# tire to road coefficient of friction, unitless
u_tire = 1.5

# targeted max deceleration, m/s^2
a_max = u_tire * g
```

∨ Braking Loads

∨ Axle loads under braking

```
# dynamic weight transfer
Wd = (h / l) * M * a_max # N
# normal force on front axle
Wf = Wfs + Wd
# normal force on rear axle
Wr = Wrs - Wd

# Maximum braking force available in each axle (N)
F_wheel_max_front = u_tire*Wf
F_wheel_max_rear  = u_tire*Wr
```

∨ Torques and Forces to maximize braking

```

# braking torque needed to each tire limit (Nm)
Torque_front = F_wheel_max_front * tire_radius
Torque_rear = F_wheel_max_rear * tire_radius

# force needed to each master cylinder to get to brake torque needed (N)
F_front_master_cylinder = (Torque_front * Amcf) / (2 * u_pad * caliper_radius_front * pi)
F_rear_master_cylinder = (Torque_rear * Amcr) / (2 * u_pad * caliper_radius_rear * pi)

```

▼ Brake Balance

```

BBf = F_front_master_cylinder / (F_front_master_cylinder + F_rear_master_cylinder)
BBr = 1 - BBf

print(f"{BBf= }")
print(f"{BBr= }")

BBf= 0.5124119344480978
BBr= 0.48758806555190215

```

▼ Driver Force

```

# Force needed from the driver, in newtons, to reach max braking (N)
F_Driver = F_front_master_cylinder / (pedal_ratio * BBf)

# converted to lbs
F_Driver_pounds = F_Driver * 0.2248
print(f"{F_Driver_pounds= }")

# lbs/g of decel
pounds_per_g = F_Driver_pounds/u_tire

F_Driver_pounds= 121.13555299562523

```

▼ Pressure in lines

The pressure should be around 500-1000 psi in the lines to lock the wheels, otherwise the calipers are over/undersized

```

Pressure_front = F_front_master_cylinder/Amcf
Pressure_rear = F_rear_master_cylinder/Amcr

Pressure_front_psi = Pressure_front*0.000145038;
Pressure_rear_psi = Pressure_rear*0.000145038;

print(f"{Pressure_front_psi= }")
print(f"{Pressure_rear_psi= }")

Pressure_front_psi= 619.3757357693045
Pressure_rear_psi= 451.2363988507232

```

Appendix C: Rotor Heat Output Hand Calculations

$$Q_{convection} = hA(T_r - T_\infty)$$

$$Q_{conduction} = \frac{4kwt}{L}(T_r - T_\infty)$$

$$Q_{radiation} = f_v f_e \sigma A(T_r^4 - T_\infty^4)$$

$$M \cdot a = \Sigma F_{wheels} = \Sigma \left(\frac{\tau_{braking}}{R_{tire}} \right)$$

$$\Sigma \tau_{braking} = \tau_{rear\ axle} + \tau_{front\ axle} = M \cdot a \cdot R_{tire}$$

$$\tau_{front\ axle} = \frac{M \cdot a \cdot R_{tire}}{1+B.B.}$$

$$\tau_{rear\ axle} = \frac{M \cdot a \cdot R_{tire}}{1+B.B.}$$

$$\tau_{fl\ wheel} = \tau_{fr\ wheel} = \frac{M \cdot a \cdot R_{tire}}{2(1+B.B.)} = F_{caliper} \cdot r_{caliper\ eff}$$

$$F_{front\ calipers} = \frac{M \cdot a \cdot R_{tire}}{2 \cdot (1 + B.B.) \cdot r_{caliper, effective}}$$

$$F_{rear\ calipers} = \frac{M \cdot a \cdot R_{tire}}{2 \cdot \left(1 + \frac{1}{B.B.}\right) \cdot r_{caliper, effective}}$$

$$v_{rotor\ at\ caliper} = v_{car} \frac{r_{caliper}}{R_{tire}}$$

$$P_{braking} = F_{caliper} \cdot v_{rotor}$$

$$P_{braking, each\ front\ wheel} = \frac{M \cdot a \cdot v_{car}}{2 \cdot (1 + B.B.)}$$

$$P_{braking, each\ rear\ wheel} = \frac{M \cdot a \cdot v_{car}}{2 \cdot \left(1 + \frac{1}{B.B.}\right)}$$

Appendix D: Control Loop Code (C++)

```
#include <Arduino.h>
#include <Arduino_CAN.h>
#include <algorithm> // For std::max

const int brake_pressure_pin = A2;
const int speed_pin = A0;
const int lin_pot_pin = A4;
const int load_cell_pin = A5;

const int lin_act_fwd_enable = 8; // digital out
const int lin_act_rev_enable = 9; // digital out
const int lin_act_fwd_speed = 3; // must be pwm
const int lin_act_rev_speed = 6; // must be pwm
const int throttle_act = 9;

float brake_pressure_val = 0;
float load_cell_val = 0;
int current_wheel_speed_rpm = 0;
int desired_wheel_speed_rpm = 0;
int beans_needed_percent = 0;
int current_brake_pressure_psi = 0;
int desired_brake_pressure_psi = 0;
double pressure_kp = 3.0;
int current_force_reading_lbs = 0.0;

int wheel_speed_threshold_rpm = 0;
int brake_pressure_threshold_psi = 3.0;

bool canTime = false;
bool HEATING = true;

int rate = 20; // Refresh rate in Hz

const double conversion = 1000;
const int teeth_count = 35;

int start_time = 0;

int get_current_wheel_speed_rpm() {
    float sensorValue = analogRead(speed_pin);
```

```

    int rpm = static_cast<int>((sensorValue / 1024 * conversion * 60) /
teeth_count);
    return rpm;
}

int get_desired_wheel_speed_rpm() {
    if (HEATING){
        return 750;
    } else {
        return 750;
    }
}

int get_current_brake_pressure_psi() {
    float sensorValue = analogRead(brake_pressure_pin);
    int psi = static_cast<int>((((sensorValue/1024.0 * 5.0) - 0.5) / 4.0) *
1000.0);
    return psi;
}

float get_current_lin_pot_volts() {
    float sensorValue = analogRead(lin_pot_pin);
    float volts = (sensorValue/1024.0 * 5.0);
    return volts;
}

int get_desired_brake_pressure_psi(float temp, float target_temp) {
    float cool_temp = 60.0;
    if (HEATING && temp < target_temp) {
        return 25;
    } else if (HEATING && temp >= target_temp){
        HEATING = false;
        return 10;
    } else if (!HEATING && temp < cool_temp){
        HEATING = true;
        return 25;
    } else {
        HEATING = false;
        return 10;
    }
}

void setup() {

```

```

Serial.begin(9600);
if (!CAN.begin(CanBitRate::BR_1000k)){
    Serial.println("CAN.begin(...) failed.");
    for (;;) {}
}
pinMode(lin_act_fwd_enable, OUTPUT);
pinMode(lin_act_rev_enable, OUTPUT);
pinMode(lin_act_fwd_speed, OUTPUT);
pinMode(lin_act_rev_speed, OUTPUT);
pinMode(throttle_act, OUTPUT);

while(get_current_lin_pot_volts() > 1){
    analogWrite(lin_act_rev_speed, 100.0);
    analogWrite(lin_act_fwd_speed, 0.0);
}

analogWrite(lin_act_rev_speed, 0.0);

current_wheel_speed_rpm = get_current_wheel_speed_rpm();
desired_wheel_speed_rpm = get_desired_wheel_speed_rpm();
if (current_wheel_speed_rpm < (desired_wheel_speed_rpm -
wheel_speed_threshold_rpm)) {
    beans_needed_percent = std::min(4.0 * (desired_wheel_speed_rpm -
current_wheel_speed_rpm), 100.0);
    analogWrite(throttle_act, (beans_needed_percent/100.0)*255.0);
} else {
    beans_needed_percent = 0.0;
    analogWrite(throttle_act, 0.0);
}

delay(5000);
}

void parseBrakeData(long id, byte data[8]) {
    switch (id) {
        case 0x4C9:
            for (int i = 0; i < 4; i++) {
                brake_msg.front_left[i] = (((short)data[2 * i]) << 8) |
data[2 * i + 1]) / 10.0 - 100.0;
            }
            break;
        case 0x4CA:
            for (int i = 0; i < 4; i++) {

```

```

        brake_msg.front_left[4 + i] = (((short)data[2 * i]) << 8)
| data[2 * i + 1]) / 10.0 - 100.0;
    }
    break;
    case 0x4CB:
        for (int i = 0; i < 4; i++) {
            brake_msg.front_left[8 + i] = (((short)data[2 * i]) << 8)
| data[2 * i + 1]) / 10.0 - 100.0;
        }
        break;
    case 0x4CC:
        for (int i = 0; i < 4; i++) {
            brake_msg.front_left[12 + i] = (((short)data[2 * i]) << 8)
| data[2 * i + 1]) / 10.0 - 100.0;
        }
        break;
    case 0x4CD:
        brake_msg.front_left_sensor_temp = (((short)data[0]) << 8) |
data[1]);
        break;
    default:
        Serial.print("Unhandled CAN ID: 0x");
        Serial.println(id, HEX);
        break;
}
}

void write_lin_act_speed_and_direction(bool forward, float speed_percent){
    if (forward) {
        digitalWrite(lin_act_rev_enable, LOW);
        analogWrite(lin_act_rev_speed, 0.0);

        digitalWrite(lin_act_fwd_enable, HIGH);
        analogWrite(lin_act_fwd_speed, (speed_percent/100.0)*255.0);
    } else {
        digitalWrite(lin_act_fwd_enable, LOW);
        analogWrite(lin_act_fwd_speed, 0.0);

        digitalWrite(lin_act_rev_enable, HIGH);
        analogWrite(lin_act_rev_speed, -1.0*(speed_percent/100.0)*255.0);
    }
}
}

```

```

void stop_lin_act(){
    digitalWrite(lin_act_rev_enable, LOW);
    analogWrite(lin_act_rev_speed, 0.0);

    digitalWrite(lin_act_fwd_enable, LOW);
    analogWrite(lin_act_fwd_speed, 0.0);
}

int get_current_force_lbs(){
    float sensorValue = (analogRead(load_cell_pin)/1024.0) * 5.0;
    int lbs = static_cast<int>(((sensorValue / 30.0) * 1500.0));
    return lbs;
}

void loop() {
    if (CAN.available()) {
        CanMsg msg = CAN.read();
        parseBrakeData(msg.id, msg.data);

        float sum = 0;
        float avg_temp = 0;
        for (int i = 0; i < 16; i++) {
            sum += brake_msg.front_left[i];
        }
        avg_temp = sum / 16.0;

        current_wheel_speed_rpm = get_current_wheel_speed_rpm();
        desired_wheel_speed_rpm = get_desired_wheel_speed_rpm();
        if (current_wheel_speed_rpm < (desired_wheel_speed_rpm -
wheel_speed_threshold_rpm)) {
            beans_needed_percent = std::min(10.0 * (desired_wheel_speed_rpm -
current_wheel_speed_rpm), 100.0);
            analogWrite(throttle_act, (beans_needed_percent/100.0)*255.0);
        } else {
            beans_needed_percent = 0.0;
            analogWrite(throttle_act, 0.0);
        }

        float target_temp = 85.0;
        current_brake_pressure_psi = get_current_brake_pressure_psi();
        desired_brake_pressure_psi = get_desired_brake_pressure_psi(avg_temp,
target_temp);
        if (current_brake_pressure_psi < desired_brake_pressure_psi -

```

```

brake_pressure_threshold_psi) {
    if (get_current_lin_pot_volts() < 3.9){
        write_lin_act_speed_and_direction(true,
std::min(pressure_kp*(desired_brake_pressure_psi -
current_brake_pressure_psi), 100.0));
    } else {
        stop_lin_act();
    }
} else if (current_brake_pressure_psi > desired_brake_pressure_psi +
brake_pressure_threshold_psi) {
    if (get_current_lin_pot_volts() > 0.7) {
        write_lin_act_speed_and_direction(false,
std::min(pressure_kp*(current_brake_pressure_psi -
desired_brake_pressure_psi), 100.0));
    } else {
        stop_lin_act();
    }
} else {
    stop_lin_act();
}

current_force_reading_lbs = get_current_force_lbs();
uint64_t extendedMillis = millis();
all_data.time = extendedMillis;
all_data.avg_brake_temp_c = avg_temp;
all_data.rpm = current_wheel_speed_rpm;
all_data.load_lbs = current_force_reading_lbs;
all_data.pressure_psi = current_brake_pressure_psi;
Serial.write((uint8_t *) &all_data, sizeof(all_data));
}
}

```

Appendix E: Serial Receiving and Chart Generation Code (Python)

```
import matplotlib.pyplot as plt
import serial
import time
import scipy.io
from struct import unpack

# Setup serial connection
ser = serial.Serial('/dev/cu.usbmodem14401', 9600)
time.sleep(2) # wait for connection to establish

first_timestamp = -1

data = {
    'timestamps': [],
    'wheel_speeds': [],
    'brake_pressures': [],
    'forces': [],
    'temperatures': []
}

try:
    while True:
        line = ser.read(size=24)
        if line:
            (timestamp, temp, speed, force, pressure) = unpack('<Qfiii',
line)

            if first_timestamp == -1:
                first_timestamp = timestamp
            data['timestamps'].append((timestamp - first_timestamp) /
1000.0)

            data['wheel_speeds'].append(speed)
            data['brake_pressures'].append(pressure)
            data['forces'].append(force)
            data['temperatures'].append(temp)
            print(temp)
except KeyboardInterrupt:

scipy.io.savemat('/Users/davidmead/Desktop/BrakeDynoControls/data_mats/run_
6.mat', data)
    ser.close()
```

```
# Plotting
plt.figure()
plt.subplot(411)
plt.plot(data['timestamps'], data['wheel_speeds'], label='Wheel Speed
(RPM)')
plt.legend()

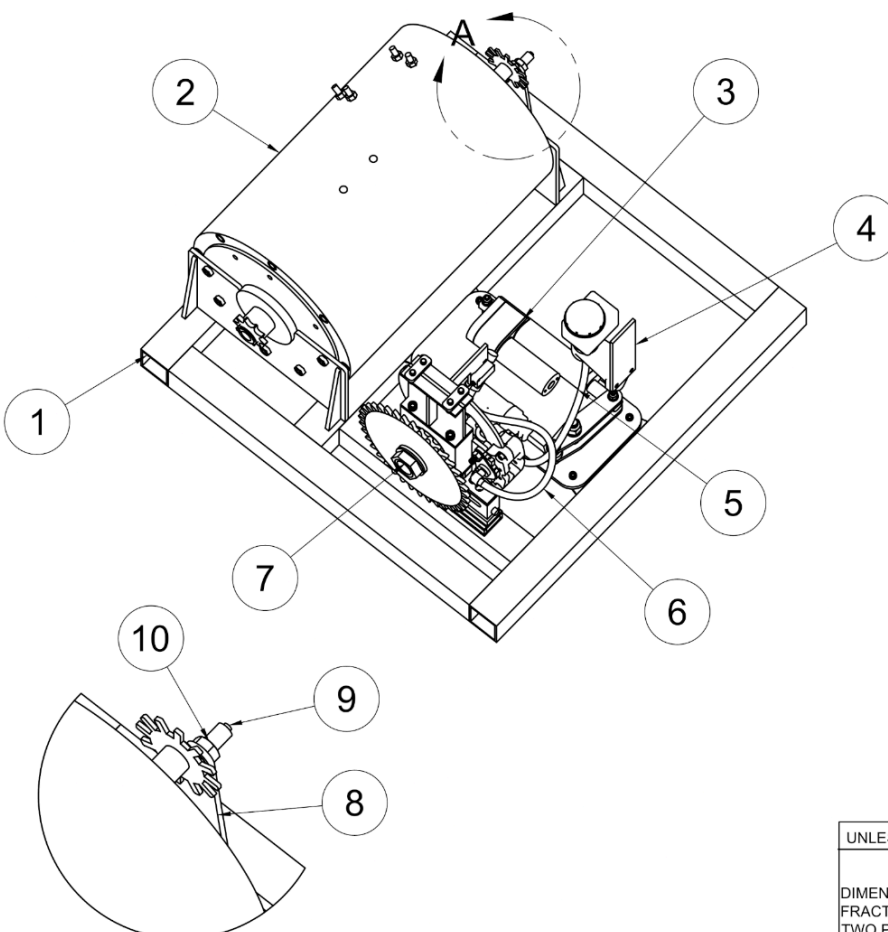
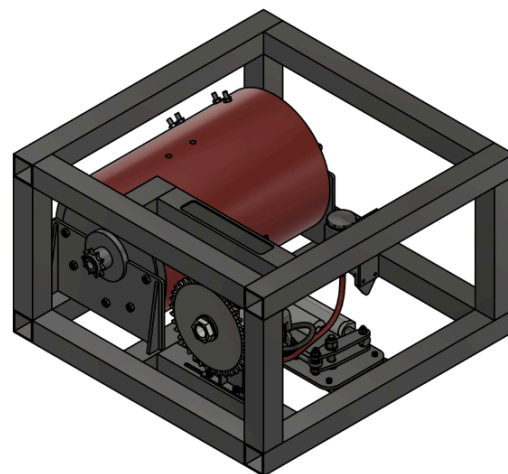
plt.subplot(412)
plt.plot(data['timestamps'], data['brake_pressures'], label='Brake Pressure
(PSI)')
plt.legend()

plt.subplot(413)
plt.plot(data['timestamps'], data['forces'], label='Force (lbs)')
plt.legend()

plt.subplot(414)
plt.plot(data['timestamps'], data['temperatures'], label='Temperature')
plt.legend()

plt.show()
```

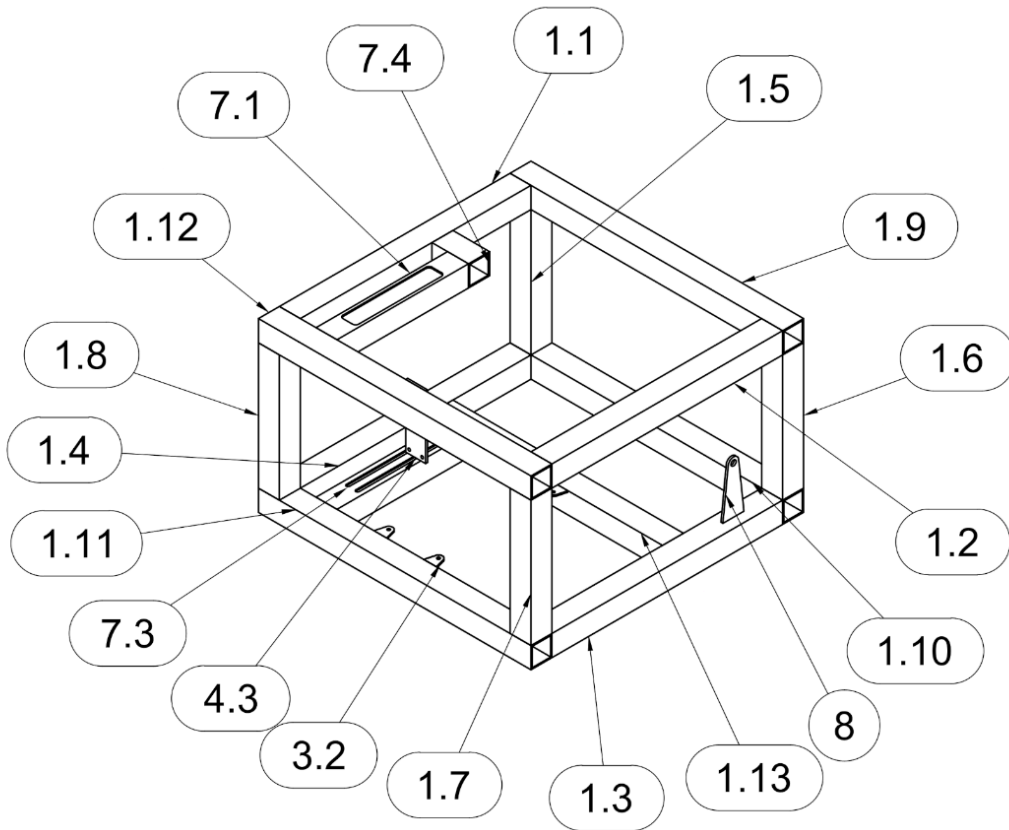
Appendix F: Detailed Drawings

| PARTS LIST | | | PARTS LIST | | |
|------------|-----|--------------------------|------------|-----|-------------------------|
| ITEM | QTY | PART NUMBER | ITEM | QTY | PART NUMBER |
| 8 | 1 | HALL EFFECT SENSOR MOUNT | 1 | 1 | FRAME |
| 9 | 1 | HALL EFFECT SENSOR | 2 | 1 | MOTOR ASSEMBLY |
| 10 | 2 | 1/2" - 20 JAM NUT | 3 | 1 | VIRTUAL PETAL MOUNTS |
| | | | 4 | 1 | BRAKE RESERVOIR 4OZ ASM |
| | | | 5 | 1 | BRAKE RESEVOIR HOSE |
| | | | 6 | 1 | BRAKE LINE |
| | | | 7 | 1 | UPRIGHT |

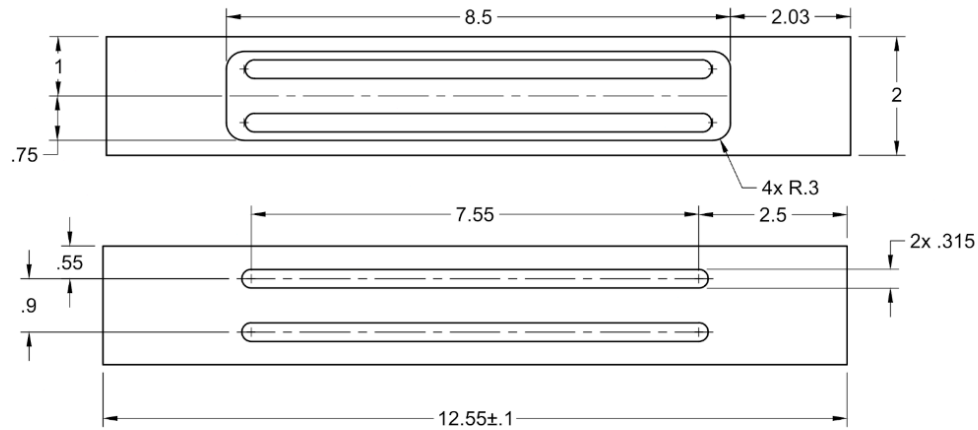
| | | | |
|--|--------------|------------------------------------|------------|
| UNLESS OTHERWISE SPECIFIED | | PROJECT | |
| DIMENSIONS ARE IN INCHES FRACTIONAL: $\pm 1/16"$ TWO PLACE DECIMAL: ± 0.01 THREE PLACE DECIMAL: ± 0.005 | | Brake Dyno | |
| | | TITLE | |
| | | BRAKE DYNO GENERAL ASSEMBLY | |
| APPROVED | SIZE | CODE | DWG NO |
| CHECKED | B | | |
| DRAWN | Ivan Pudwill | 10/31/2023 | SCALE 1:10 |
| | | | WEIGHT |
| | | | SHEET 1/3 |

DETAIL A
SCALE 1:3

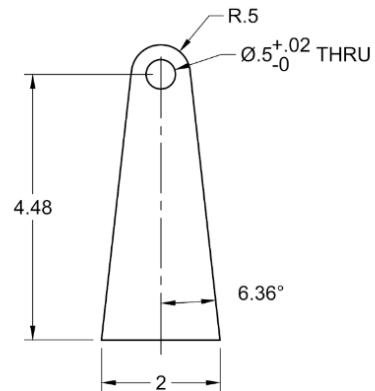


| PARTS LIST | | | |
|------------|-----|--------------------------|-------------------------------|
| ITEM | QTY | PART NUMBER | DESCRIPTION |
| 1 | 1 | FRAME | |
| 1.1 | 1 | UPPER_FRONT | SHS 2" X .12" WALL X 22" L |
| 1.2 | 1 | UPPER_BACK | SHS 2" X .12" WALL X 22" L |
| 1.3 | 1 | LOWER_BACK | SHS 2" X .12" WALL X 22" L |
| 1.4 | 1 | LOWER_FRONT | SHS 2" X .12" WALL X 22" L |
| 1.5 | 1 | FRONT_LEFT_VERT | SHS 2" X .12" WALL X 12" L |
| 1.6 | 1 | BACK_LEFT_VERT | SHS 2" X .12" WALL X 12" L |
| 1.7 | 1 | BACK_RIGHT_VERT | SHS 2" X .12" WALL X 12" L |
| 1.8 | 1 | FRONT_RIGHT_VERT | SHS 2" X .12" WALL X 12" L |
| 1.9 | 1 | UPPER_LEFT | SHS 2" X .12" WALL X 26" L |
| 1.10 | 1 | LOWER_LEFT | SHS 2" X .12" WALL X 26" L |
| 1.11 | 1 | LOWER_RIGHT | SHS 2" X .12" WALL X 26" L |
| 1.12 | 1 | UPPER_RIGHT | SHS 2" X .12" WALL X 26" L |
| 1.13 | 1 | MOTOR_SUPPORT | SHS 2" X .12" WALL X 22" L |
| 3 | 1 | VIRTUAL PETAL MOUNTS | |
| 3.2 | 4 | VIRTUAL PEDAL MOUNT | 1/8" STEEL |
| 4 | 1 | BRAKE RESERVOIR 4OZ ASM | |
| 4.3 | 1 | BRAKE RESERVOIR MOUNT | 3/16" STEEL |
| 7 | 1 | UPRIGHT | |
| 7.1 | 1 | UPPER_MOUNT_TUBE | SHS 2" X .12" WALL X 12.55" L |
| 7.3 | 1 | LOWER_MOUNT_TUBE | SHS 2" X .12" WALL X 12.55" L |
| 7.4 | 1 | UPPER_SUPPORT | SHS 2" X .12" WALL X 4" L |
| 8 | 1 | HALL EFFECT SENSOR MOUNT | 1/16" STEEL |

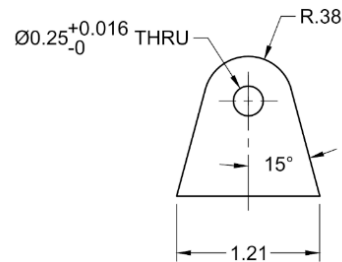
| | | | | | |
|--|--------------|---|------------|--------|-----------|
| UNLESS OTHERWISE SPECIFIED | | PROJECT | | | |
| DIMENSIONS ARE IN INCHES FRACTIONAL: ± 1/16" TWO PLACE DECIMAL: ± 0.01 THREE PLACE DECIMAL: ± 0.005 | | Brake Dyno TITLE FRAME ASSEMBLY | | | |
| | | APPROVED | SIZE | CODE | DWG NO |
| CHECKED | B | | | | A |
| DRAWN | Ivan Pudwill | 10/31/2023 | SCALE 1:10 | WEIGHT | SHEET 2/3 |



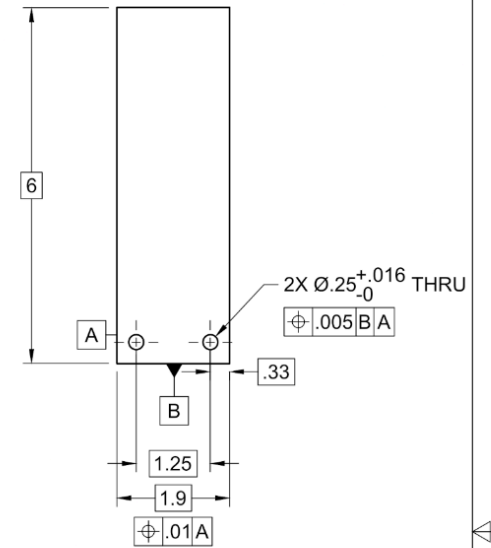
(7.1/7.3) UPRIGHT SUPPORT TUBE



(8) HALL EFFECT SENSOR MOUNT

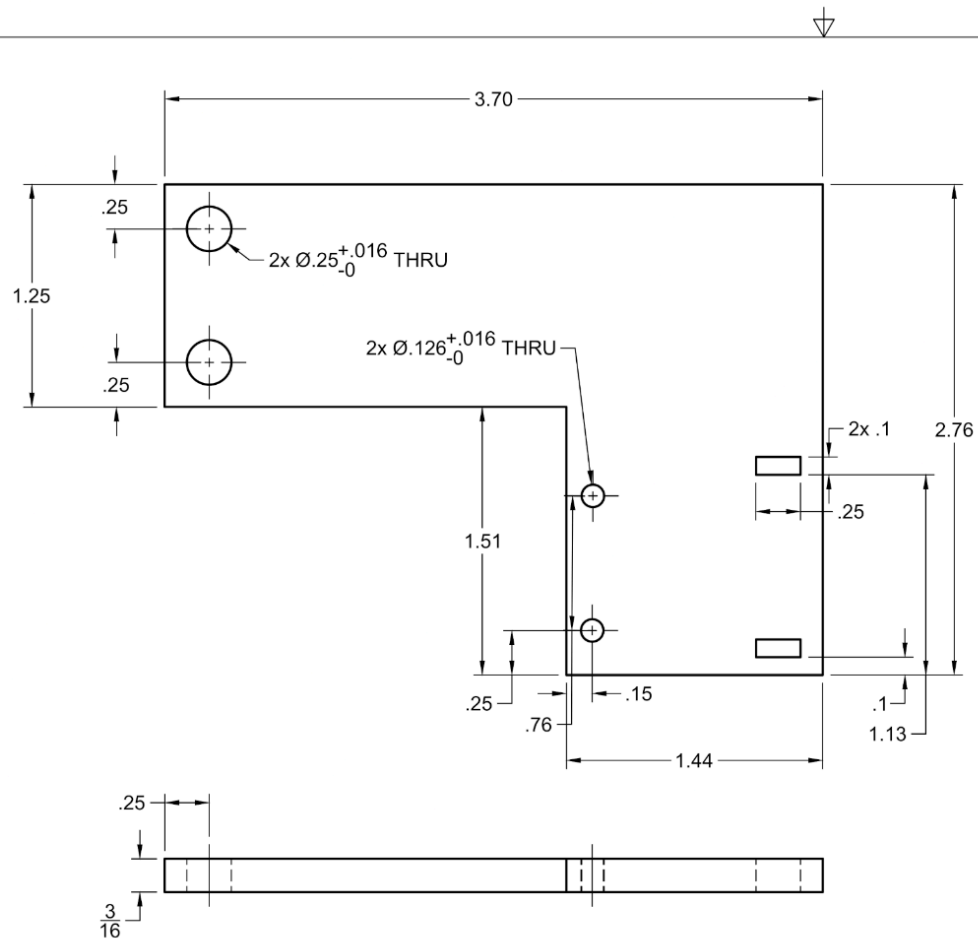


(3.2) VIRTUAL PEDAL MOUNT

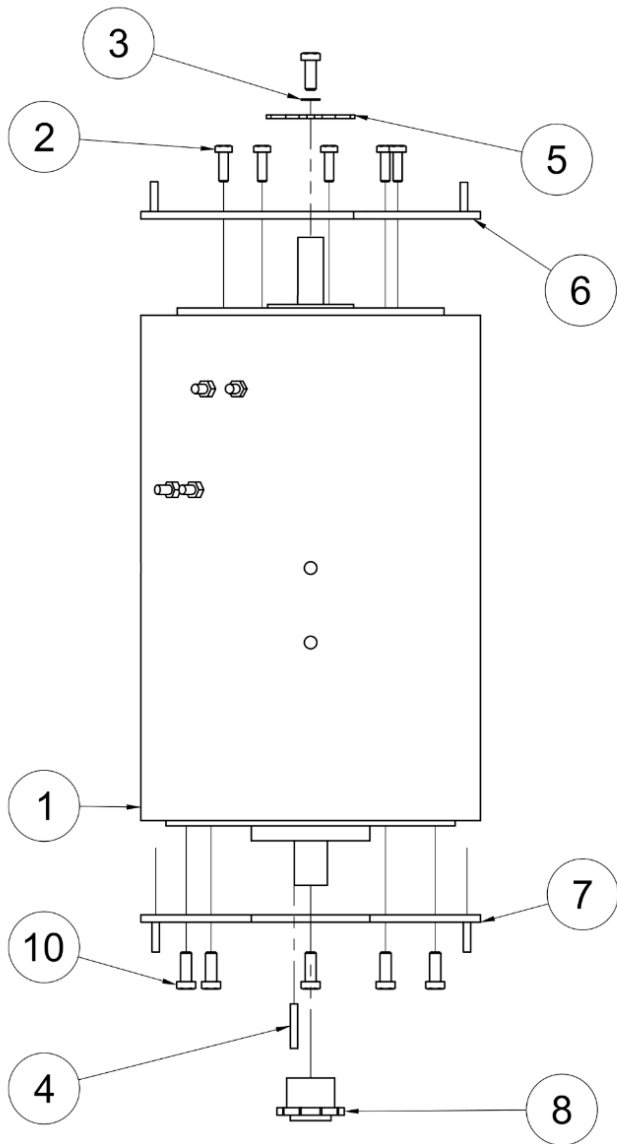


BRAKE RESERVOIR MOUNT

| | | | | |
|--|--------------|------------------------------|-------------------------|-----------|
| UNLESS OTHERWISE SPECIFIED | | PROJECT | | |
| DIMENSIONS ARE IN INCHES FRACTIONAL: ± 1/16" TWO PLACE DECIMAL: ± 0.01 THREE PLACE DECIMAL: ± 0.005 | | Brake Dyno | | |
| | | TITLE MISC MOUNT DRAWINGS | | |
| APPROVED | SIZE | CODE | DWG NO | REV |
| CHECKED | B | | | A |
| DRAWN | Ivan Pudwill | 10/31/2023 | SCALE 1:2 (From parent) | WEIGHT |
| | | | | SHEET 3/3 |

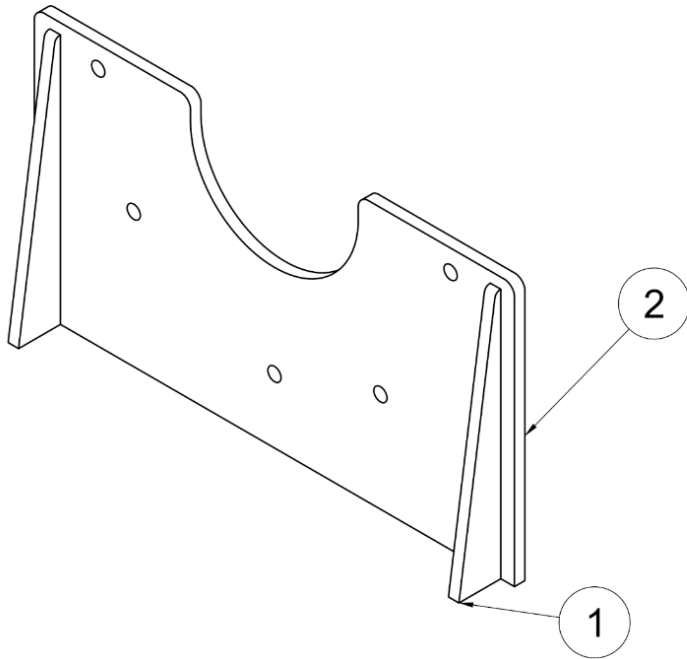


| | | | | | |
|----------|------------|----------------------|-----------|--------|-----------|
| | | PROJECT | | | REV |
| | | Brake Dyno | | | |
| | | TITLE | | | A |
| | | IR TEMP SENSOR MOUNT | | | |
| APPROVED | SIZE | CODE | DWG NO | | |
| CHECKED | B | | | | |
| DRAWN | David Mead | 10/30/23 | SCALE 1:2 | WEIGHT | SHEET 1/1 |



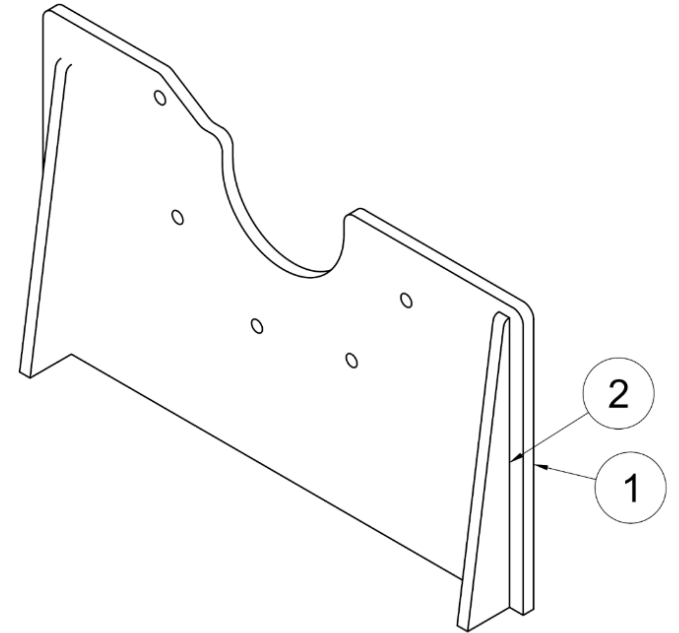
| PARTS LIST | | | |
|------------|-----|------------------------------|--------------------------------|
| ITEM | QTY | PART NUMBER | DESCRIPTION |
| 1 | 1 | WARP11 | NETGAIN MOTORS WARP11 DC MOTOR |
| 2 | 5 | 5/16" - 18 X 1" GRADE 8 BOLT | |
| 3 | 1 | 3/8" - 16 18-8 SS WASHER | |
| 4 | 1 | DRIVE KEY | 1/4" X 1/4" X 1" SQUARE KEY |
| 5 | 1 | TONE RING | 1/8" STEEL |
| 6 | 1 | COMM SIDE MOUNTING PLATE | 1/4" STEEL WELDMENT |
| 7 | 1 | DRIVE SIDE MOUNTING PLATE | 1/4" STEEL WELDMENT |
| 8 | 1 | 10 TOOTH SPROCKET | 520 ROLLER CHAIN SPROCKET |
| 10 | 6 | 3/8" -16 X 1" GRADE 8 BOLT | |

| | | | | | |
|--|--------------|---|-----------|--------|-----------|
| UNLESS OTHERWISE SPECIFIED | | PROJECT | | | |
| DIMENSIONS ARE IN INCHES TOLERANCES: XXX ± XXX FRACTIONAL: XXX ± XXX TWO PLACE DECIMAL: XXX ± XXX THREE PLACE DECIMAL: XXX ± XXX | | Brake Dyno TITLE Motor Assembly | | | |
| | | SIZE | CODE | DWG NO | REV |
| APPROVED | | B | | | A |
| CHECKED | | | | | |
| DRAWN | Ivan Pudwill | 10/30/2023 | SCALE 1:5 | WEIGHT | SHEET 1/5 |



| PARTS LIST | | | |
|------------|-----|-----------------|-------------|
| ITEM | QTY | PART NUMBER | DESCRIPTION |
| 1 | 2 | END PLATE RIB | 1/4" STEEL |
| 2 | 1 | DRIVE END PLATE | 1/4" STEEL |

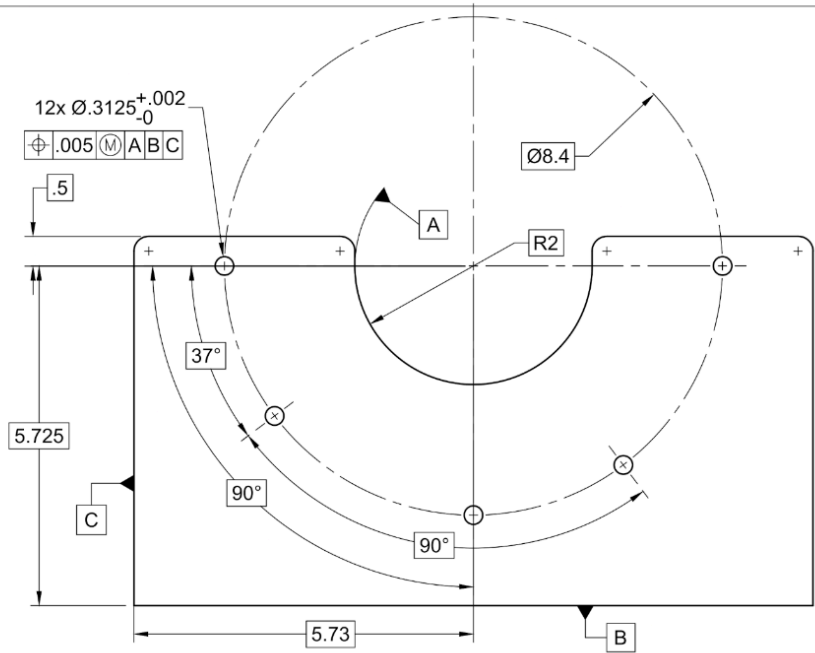
(7) DRIVE END MOUNT PLATE WELDMENT



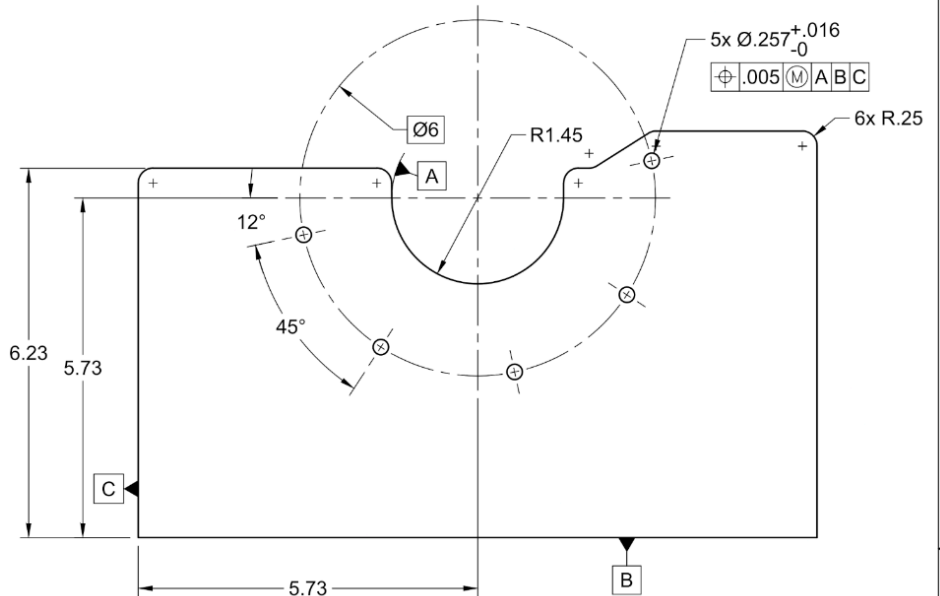
| PARTS LIST | | | |
|------------|-----|----------------|-------------|
| ITEM | QTY | PART NUMBER | DESCRIPTION |
| 1 | 1 | COMM END PLATE | 1/4" STEEL |
| 2 | 2 | END PLATE RIB | 1/4" STEEL |

(6) COMM END MOUNT PLATE WELDMENT

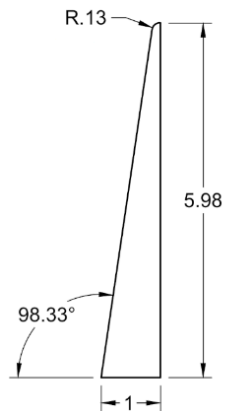
| | | | | |
|--|--------------|---|-----------|--------|
| UNLESS OTHERWISE SPECIFIED | | PROJECT | | |
| DIMENSIONS ARE IN INCHES TOLERANCES: XXX ± XXX FRACTIONAL: XXX ± XXX TWO PLACE DECIMAL: XXX ± XXX THREE PLACE DECIMAL: XXX ± XXX | | Brake Dyno | | |
| | | TITLE Mounting Plates Welded Assembly | | |
| APPROVED | SIZE | CODE | DWG NO | REV |
| CHECKED | B | | | A |
| DRAWN | Ivan Pudwill | 10/30/2023 | SCALE 1:4 | WEIGHT |
| | | | SHEET 2/5 | |



(7.1) DRIVE END MOUNT PLATE

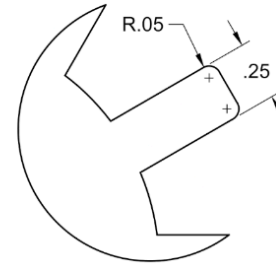
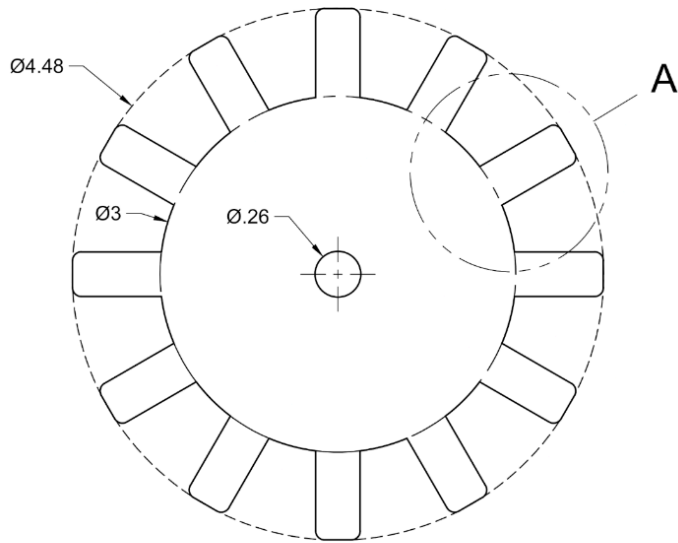


(6.1) DRIVE END MOUNT PLATE



(6.2/7.2) END PLATE RIB

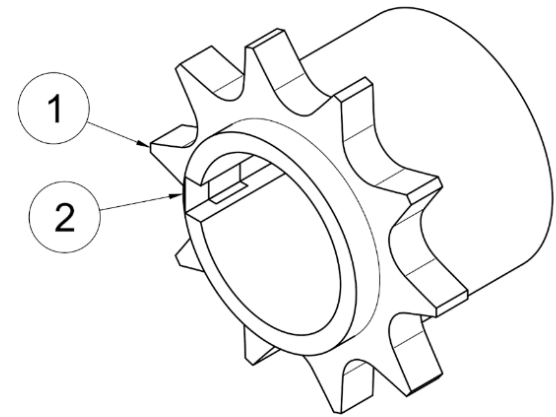
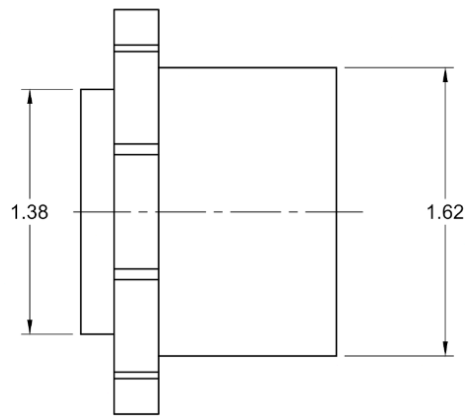
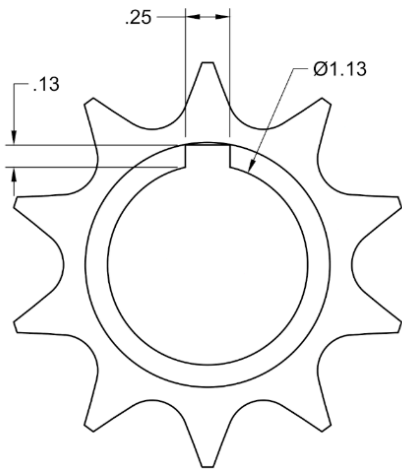
| | | | | |
|--|--------------|---|-----------|----------|
| UNLESS OTHERWISE SPECIFIED | | PROJECT | | |
| DIMENSIONS ARE IN INCHES TOLERANCES: XXX ± XXX FRACTIONAL: XXX ± XXX TWO PLACE DECIMAL: XXX ± XXX THREE PLACE DECIMAL: XXX ± XXX | | Brake Dyno | | |
| | | TITLE (6)/(7) Mounting Plates Drawing | | |
| | | APPROVED | SIZE | CODE |
| CHECKED | B | | | REV A |
| DRAWN | Ivan Pudwill | 10/30/2023 | SCALE 1:2 | WEIGHT |
| | | | SHEET 3/5 | |



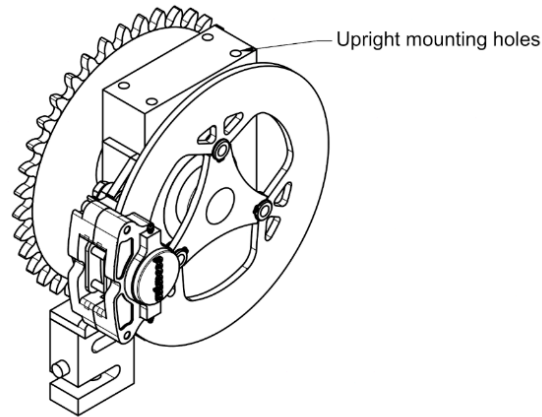
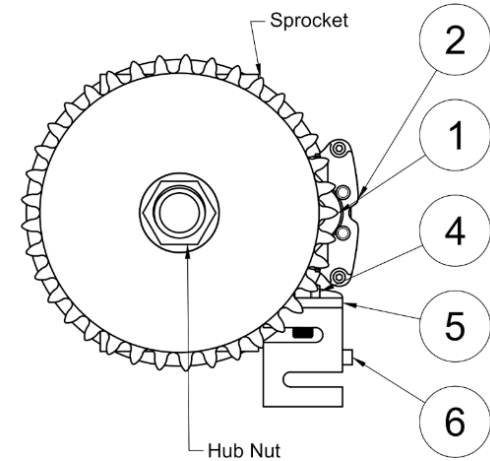
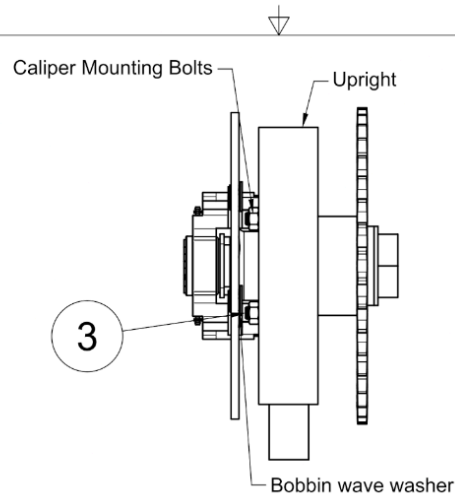
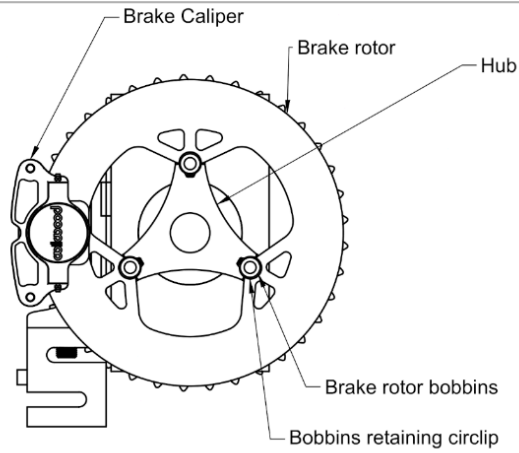
DETAIL A
SCALE 2:1

| | | | | |
|--|--------------|-------------------------------|-------------|--------|
| UNLESS OTHERWISE SPECIFIED | | PROJECT | | |
| DIMENSIONS ARE IN INCHES TOLERANCES: XXX ± XXX FRACTIONAL: XXX ± XXX TWO PLACE DECIMAL: XXX ± XXX THREE PLACE DECIMAL: XXX ± XXX | | Brake Dyno | | |
| | | TITLE (5) TONE RING | | |
| APPROVED | SIZE | CODE | DWG NO | REV |
| CHECKED | B | | | A |
| DRAWN | Ivan Pudwill | 10/30/2023 | SCALE 1.5:1 | WEIGHT |
| | | | SHEET 4/5 | |

| PARTS LIST | | | |
|------------|-----|--|---|
| ITEM | QTY | PART NUMBER | DESCRIPTION |
| 1 | 1 | 10 TOOTH SPROCKET | OEM 10 TOOTH 520 SPROCKET |
| 2 | 1 | HUBX1-1/8 - X SERIES WELD ON HUB 1-1/8" BORE | MODIFIED-HUBX1-1/8 - X SERIES WELD ON HUB 1-1/8" BORE |

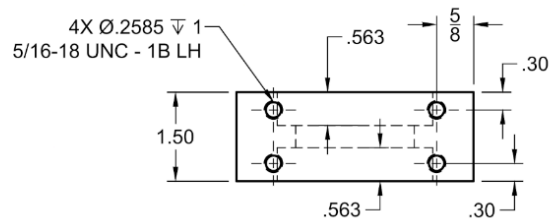
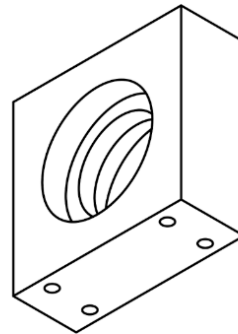
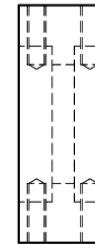
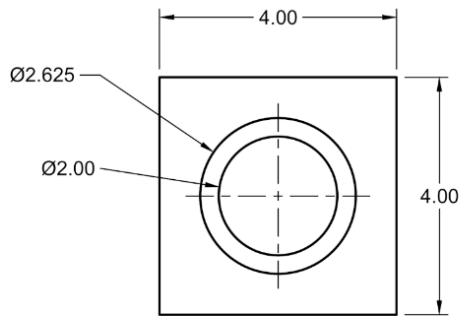


| | | | | |
|--|--------------|---------------------------------------|-----------|-----------|
| UNLESS OTHERWISE SPECIFIED | | PROJECT | | |
| DIMENSIONS ARE IN INCHES TOLERANCES: XXX ± XXX FRACTIONAL: XXX ± XXX TWO PLACE DECIMAL: XXX ± XXX THREE PLACE DECIMAL: XXX ± XXX | | Brake Dyno | | |
| | | TITLE (8) Sprocket Assembly | | |
| APPROVED | SIZE | CODE | DWG NO | REV |
| CHECKED | B | | | A |
| DRAWN | Ivan Pudwill | 10/30/2023 | SCALE 1:1 | WEIGHT |
| | | | | SHEET 5/5 |

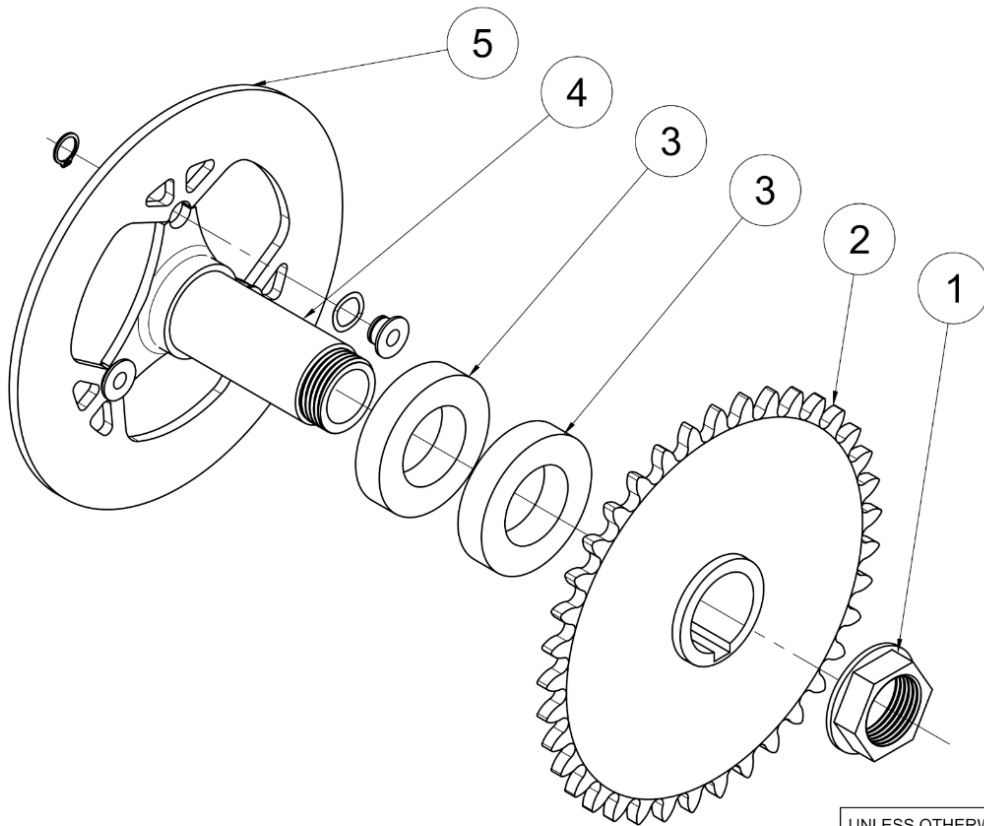


| 6 | 1 | OP-312 LOAD CELL |
|------------|-----|--|
| 5 | 1 | COMPONENT12(MIRROR) |
| 4 | 1 | 92620A744_ZINC YELLOW-CHROMATE PLATED HEX HEAD SCREW(MIRROR) |
| 3 | 1 | FASTENERS |
| 2 | 1 | WILWOOD GP200 |
| 1 | 1 | HUB |
| ITEM | QTY | PART NUMBER |
| PARTS LIST | | |

| UNLESS OTHERWISE SPECIFIED | | PROJECT | | |
|--|---------|--------------------------------|--------|-----------|
| DIMENSIONS ARE IN INCHES TOLERANCES: XXX ± XXX FRACTIONAL: XXX ± XXX TWO PLACE DECIMAL: XXX ± XXX THREE PLACE DECIMAL: XXX ± XXX | | BrakeDyno | | |
| | | TITLE Wheel Assembly | | |
| APPROVED | SIZE | CODE | DWG NO | REV |
| CHECKED | B | | | A |
| DRAWN David Mead | 10/9/23 | SCALE 1:3 | WEIGHT | SHEET 1/1 |

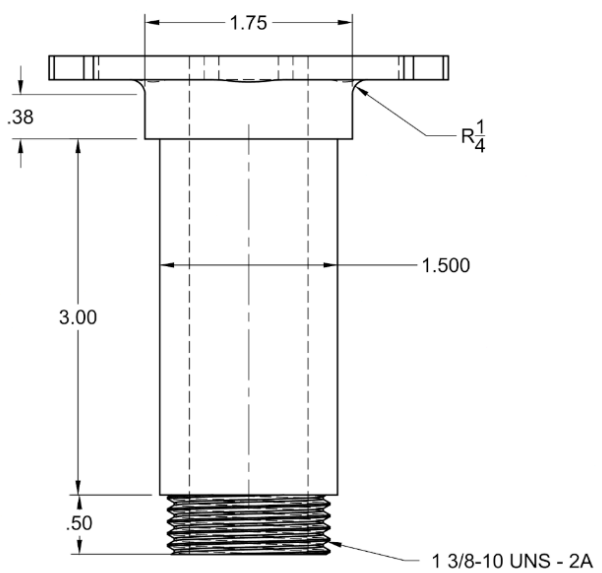
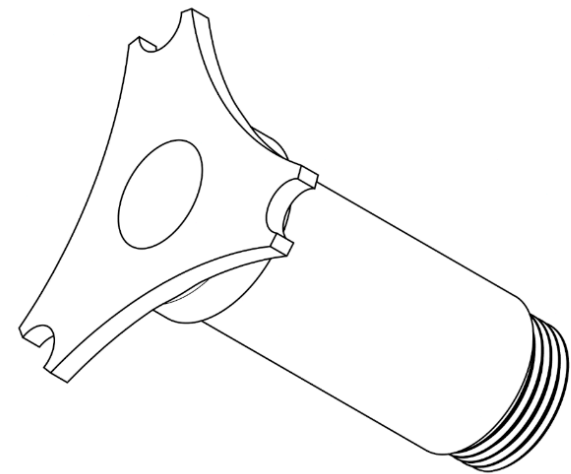
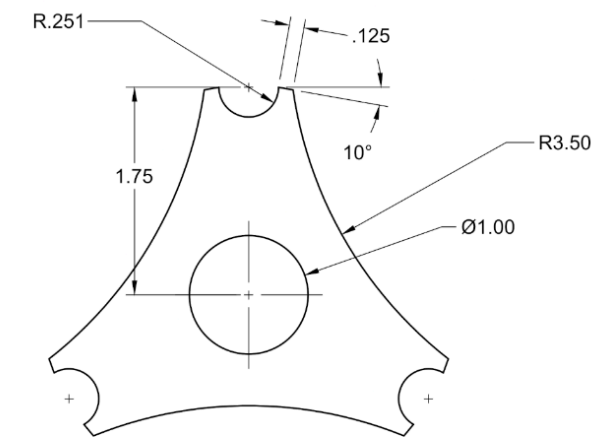


| | | | | | |
|----------|------------|------------|-----------|--------|-----------|
| | | PROJECT | | | REV |
| | | Brake Dyno | | | |
| | | TITLE | | | A |
| | | Upright | | | |
| APPROVED | SIZE | CODE | DWG NO | | |
| CHECKED | B | | | | |
| DRAWN | David Mead | 10/30/23 | SCALE 1:2 | WEIGHT | SHEET 1/1 |

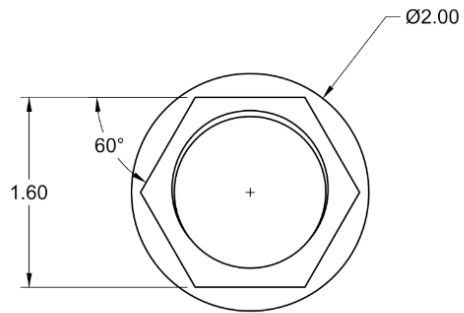


| PARTS LIST | | |
|------------|-----|-------------------|
| ITEM | QTY | PART NUMBER |
| 1 | 1 | NUT |
| 2 | 1 | 37 TOOTH SPROCKET |
| 3 | 2 | R24 BEARING |
| 4 | 1 | HUB |
| 5 | 1 | BRAKE ROTOR |

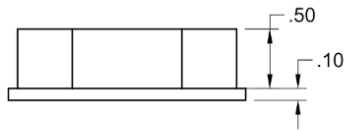
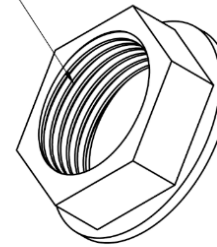
| | | | | |
|--|----------|------------------------------|--------|-----------|
| UNLESS OTHERWISE SPECIFIED | | PROJECT | | |
| DIMENSIONS ARE IN INCHES TOLERANCES: XXX ± XXX FRACTIONAL: XXX ± XXX TWO PLACE DECIMAL: XXX ± XXX THREE PLACE DECIMAL: XXX ± XXX | | Brake Dyno | | |
| | | TITLE Hub Assembly | | |
| APPROVED | SIZE | CODE | DWG NO | REV |
| CHECKED | B | | | A |
| DRAWN David Mead | 10/18/23 | SCALE 1:2 | WEIGHT | SHEET 1/1 |



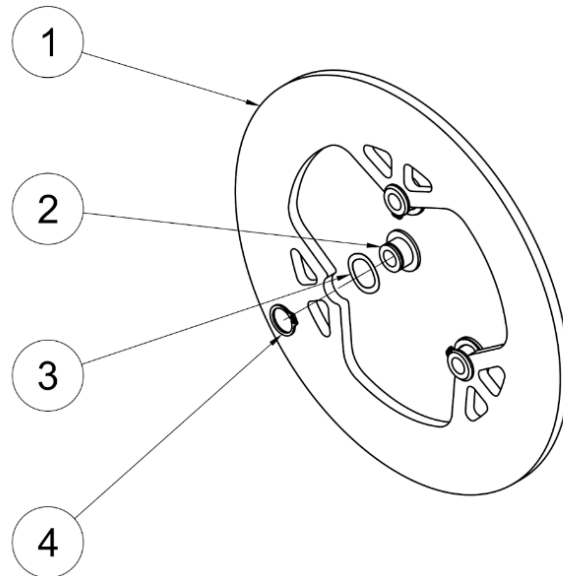
| | | | | | |
|--|------------|---------------------------------|-------------|-----------|--------|
| UNLESS OTHERWISE SPECIFIED | | PROJECT | | | |
| DIMENSIONS ARE IN INCHES TOLERANCES: XXX ± XXX FRACTIONAL: XXX ± XXX TWO PLACE DECIMAL: XXX ± XXX THREE PLACE DECIMAL: XXX ± XXX | | Brake Dyno | | | |
| | | TITLE (4) Hub Drawing | | | |
| | | APPROVED | SIZE | CODE | DWG NO |
| | | CHECKED | B | | |
| DRAWN | David Mead | 10/18/23 | SCALE 1:1.5 | WEIGHT | |
| | | | | SHEET 1/1 | |
| | | | | REV A | |



1 3/8-10 UNS - 2B

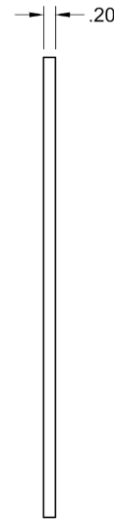
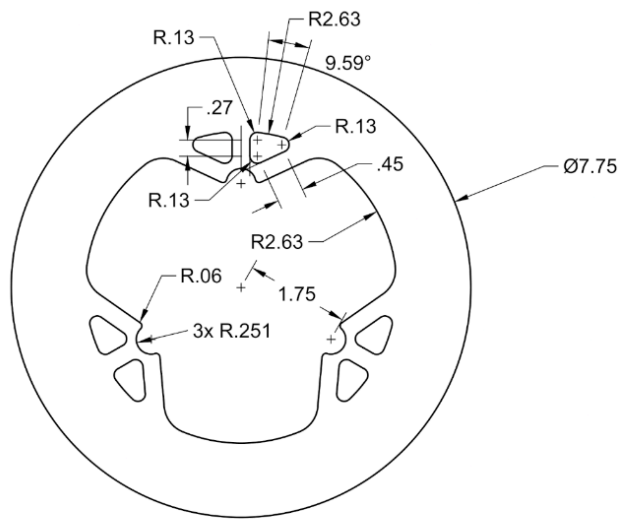


| | | | | |
|--|------------|---------------------------------|-----------|--------|
| UNLESS OTHERWISE SPECIFIED | | PROJECT | | |
| DIMENSIONS ARE IN INCHES TOLERANCES: XXX ± XXX FRACTIONAL: XXX ± XXX TWO PLACE DECIMAL: XXX ± XXX THREE PLACE DECIMAL: XXX ± XXX | | Brake Dyno | | |
| | | TITLE (1) Nut Drawing | | |
| APPROVED | SIZE | CODE | DWG NO | REV |
| CHECKED | B | | | A |
| DRAWN | David Mead | 10/18/23 | SCALE 1 | WEIGHT |
| | | | SHEET 1/1 | |

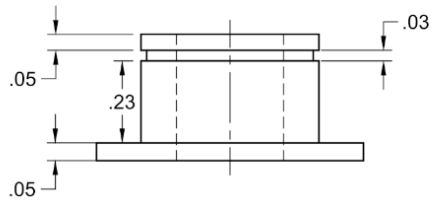
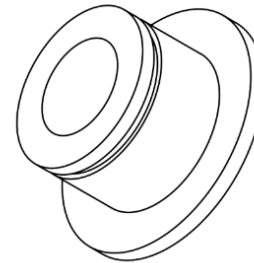
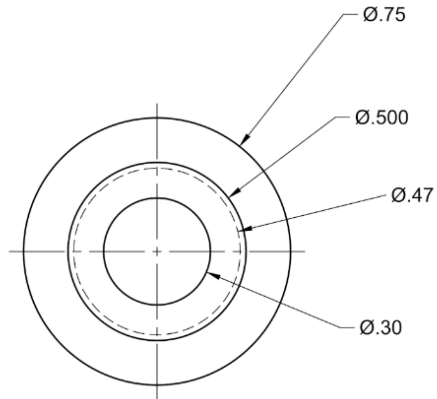


| PARTS LIST | | | |
|------------|-----|----------------------------|-----------------------------|
| ITEM | QTY | PART NUMBER | MATERIAL |
| 1 | 1 | ROTOR | STEEL AISI 4130 259 QT |
| 2 | 3 | BOBBIN | TITANIUM 6AL-4V |
| 3 | 3 | WAVE WASHER | STAINLESS STEEL AISI 302 |
| 4 | 3 | EXTERNAL RETAINING RING | STEEL AISI 1060 |

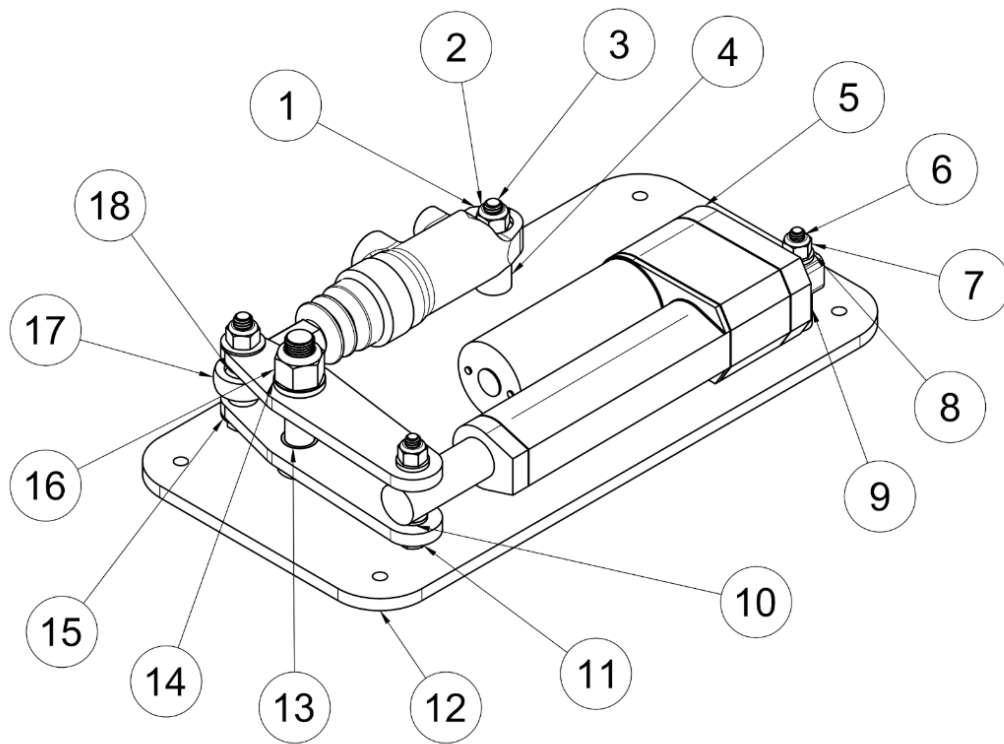
| | | | | |
|--|-----------|--------------------------------------|-----------|-----|
| UNLESS OTHERWISE SPECIFIED | | PROJECT | | |
| DIMENSIONS ARE IN INCHES TOLERANCES: XXX ± XXX FRACTIONAL: XXX ± XXX TWO PLACE DECIMAL: XXX ± XXX THREE PLACE DECIMAL: XXX ± XXX | | Brake Dyno | | |
| | | TITLE Brake Rotor Assembly | | |
| APPROVED | SIZE | CODE | DWG NO | REV |
| CHECKED | B | | | A |
| DRAWN David Mead 10/18/23 | SCALE 1:2 | WEIGHT | SHEET 1/1 | |



| | | | | |
|--|-----------|---|-----------|-----|
| UNLESS OTHERWISE SPECIFIED | | PROJECT | | |
| DIMENSIONS ARE IN INCHES TOLERANCES: XXX ± XXX FRACTIONAL: XXX ± XXX TWO PLACE DECIMAL: XXX ± XXX THREE PLACE DECIMAL: XXX ± XXX | | BrakeDyno | | |
| | | TITLE Brake Rotor Assembly (1) Brake Rotor | | |
| APPROVED | SIZE | CODE | DWG NO | REV |
| CHECKED | B | | | A |
| DRAWN David Mead 10/18/23 | SCALE 1:2 | WEIGHT | SHEET 1/1 | |

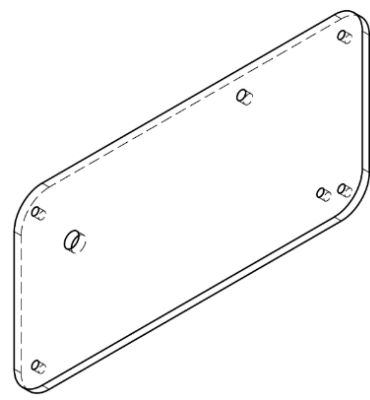
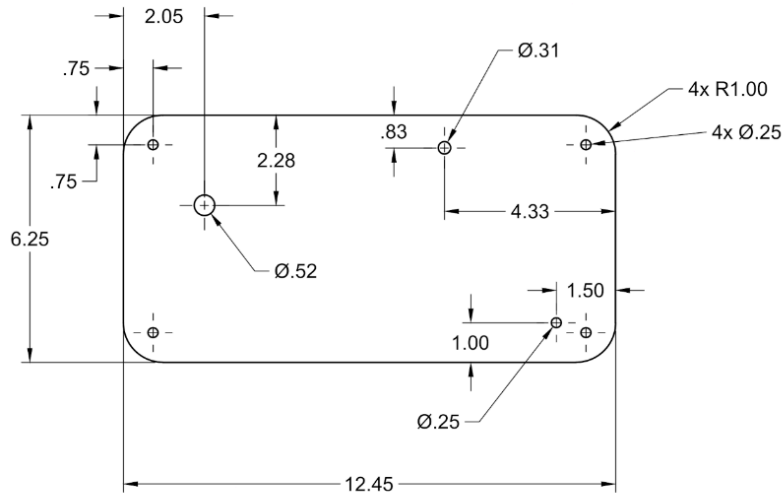


| | | | | |
|--|------------|---|-----------|--------|
| UNLESS OTHERWISE SPECIFIED | | PROJECT | | |
| DIMENSIONS ARE IN INCHES TOLERANCES: XXX ± XXX FRACTIONAL: XXX ± XXX TWO PLACE DECIMAL: XXX ± XXX THREE PLACE DECIMAL: XXX ± XXX | | Brake Dyno | | |
| | | TITLE Brake Rotor Assembly (2) Bobbins | | |
| APPROVED | SIZE | CODE | DWG NO | REV |
| CHECKED | B | | | A |
| DRAWN | David Mead | 10/18/23 | SCALE 3:1 | WEIGHT |
| | | | SHEET 1/1 | |

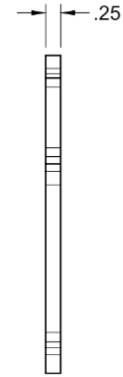
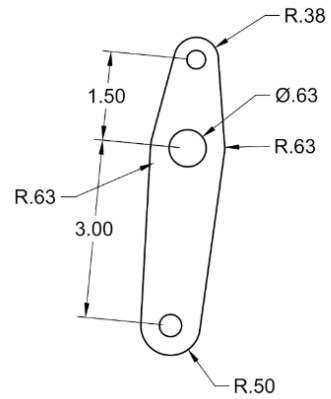


| PARTS LIST | | |
|------------|-----|------------------------------|
| ITEM | QTY | PART NUMBER |
| 1 | 1 | MASTER CYLINDER |
| 2 | 2 | 5/16-18 LOCKNUT |
| 3 | 2 | 5/16-18 BOLT |
| 4 | 1 | MASTER CYLINDER END STANDOFF |
| 5 | 1 | LINEAR ACTUATOR |
| 6 | 1 | 1/4-20 2-1/4" BOLT |
| 7 | 2 | 1/4-20 LOCKNUT |
| 8 | 4 | 1/4" WASHER |
| 9 | 1 | LINEAR ACTUATOR END STANDOFF |
| 10 | 2 | 1/4" SHAFT BUSHING |
| 11 | 1 | PIVOT |
| 12 | 1 | PLATE |
| 13 | 1 | 1/2" SHAFT BUSHING |
| 14 | 1 | 1/2" SHAFT BUSHING (1) |
| 15 | 3 | 0.344" OD WASHER |
| 16 | 1 | 1/2-20 LOCKNUT |
| 17 | 1 | BALL END JOINT |
| 18 | 1 | ROD END SPACER |
| 19 | 1 | PIVOT (1) |
| 20 | 1 | ROD END SPACER 2 |
| 21 | 1 | 1/4-20 2" BOLT |
| 22 | 1 | 1/2" WASHER |
| 23 | 1 | 1/2-20 3" BOLT |
| 24 | 1 | PIVOT STANDOFF |

| | | | | |
|--|-----------|--------------------------------|-----------|-----|
| UNLESS OTHERWISE SPECIFIED | | PROJECT | | |
| DIMENSIONS ARE IN INCHES TOLERANCES: XXX ± XXX FRACTIONAL: XXX ± XXX TWO PLACE DECIMAL: XXX ± XXX THREE PLACE DECIMAL: XXX ± XXX | | Brake Dyno | | |
| | | TITLE Pedal Assembly | | |
| APPROVED | SIZE | CODE | DWG NO | REV |
| CHECKED | B | | | A |
| DRAWN David Mead 10/18/23 | SCALE 1:2 | WEIGHT | SHEET 1/1 | |



| | | | | | |
|--|------------|---|-----------|-----------|--------|
| UNLESS OTHERWISE SPECIFIED | | PROJECT | | | |
| DIMENSIONS ARE IN INCHES TOLERANCES: XXX ± XXX FRACTIONAL: XXX ± XXX TWO PLACE DECIMAL: XXX ± XXX THREE PLACE DECIMAL: XXX ± XXX | | Brake Dyno | | | |
| | | TITLE Pedal Asembly (12) Plate | | | |
| | | APPROVED | SIZE | CODE | DWG NO |
| | | CHECKED | B | | |
| DRAWN | David Mead | 10/18/23 | SCALE 1:2 | WEIGHT | |
| | | | | SHEET 1/1 | |
| | | | | REV A | |



| | | | | |
|--|------------|--|-----------|--------|
| UNLESS OTHERWISE SPECIFIED | | PROJECT | | |
| DIMENSIONS ARE IN INCHES TOLERANCES: XXX ± XXX FRACTIONAL: XXX ± XXX TWO PLACE DECIMAL: XXX ± XXX THREE PLACE DECIMAL: XXX ± XXX | | Brake Dyno | | |
| | | TITLE Pedal Assembly (11) Pivot | | |
| APPROVED | SIZE | CODE | DWG NO | REV |
| CHECKED | B | | | A |
| DRAWN | David Mead | 10/18/23 | SCALE 1:2 | WEIGHT |
| | | | SHEET 1/1 | |

Appendix G: Video Demonstration

<https://drive.google.com/file/d/14bS4KloPCaP7xYZU19u-LxuGRLbR3LGG/view?usp=sharing>